HIGH DENSITY PLASMA ETCHING OF NOVEL ELECTRONIC AND MAGNETIC MATERIALS: $LaCaMnO_3$ AND SiC

BY

JUAN-JUAN WANG

A THESIS PRESENTED TO THE GRADUATE SCHOOL
OF THE UNIVERSITY OF FLORIDA IN PARTIAL FULFILLMENT
OF THE REQUIREMENTS FOR THE DEGREE OF
MASTER OF SCIENCE

UNIVERSITY OF FLORIDA

1998

DEDICATED TO MY HUSBAND,
YONG WU,
MY PARENTS,
YU-GUANG WANG AND
YU-HUA ZHENG,
AND MY PARENTS-IN-LAW,
JI-ZHOU WU AND
WEN-RUO YANG

ACKNOWLEDGMENTS

I would like to express my gratitude from my heart to Dr. Stephen J. Pearton, my advisor, for his encouragement, expert advice, guidance, and support throughout this project.

I would also like to express my appreciation to my committee members, Dr. Cammy R. Abernathy and Dr. Rajiv K. Singh, for their help, suggestions, and time.

Everyone in our group is greatly appreciated for their kind cooperation.

Most of all, I thank my husband, who has inspired me to work hard and been by my side throughout every step of my thesis and always encouraged me.

TABLE OF CONTENTS

LIST OF TABLES

LIST OF FIGURES

Abstract of Thesis Presented to the Graduate School
of the University of Florida in Partial Fulfillment of the
Requirements for the Degree of Master of Science

HIGH DENSITY PLASMA ETCHING OF NOVEL ELECTRONIC AND MAGNETIC MATERIALS: $LaCaMnO_3$ AND SiC

By

Juan-Juan Wang

August, 1998

Chairman: Stephen J. Pearton
Major Department: Materials Science and Engineering

New etch processes have been developed for important magnetic and electronic materials with application in next generation data storage and power switching. First, a number of different plasma chemistries have been employed for patterning of $LaCaMnO_3$ (and related SmCo) thin films for application in magnetic field-biased structures based on the colossal magneto-resistive effect. For $LaCaMnO_3$ there was no chemical enhancement in etch rate over simple Ar sputtering for Cl_2, SF_6 and CH_4/H_2 plasmas under high ion density conditions except BI_3 and BBr_3 plasmas. This is expected based on the vapor pressures of the prospective etch products. There is some chemical enhancement of etch rates at low halide compositions in the BI_3/Ar and BBr_3/Ar discharges, and the rates are a strong function of ion/neutral ratio. In this case, etch yields are typically low (<0.3) under Inductively Coupled Plasma conditions. For SmCo

however, etch rates up to 7,000 Å·min^{-1} were obtained in Cl_2/Ar plasmas, which is an order of magnitude faster than Ar sputtering under the same experimental conditions. Smooth etched surface morphologies and anistropic sidewalls were obtained for both materials over a wide range of plasma source and chuck powers.

Secondly, a parametric study of the etching characteristics of 6H p^+ and n^+ SiC and thin film $SiC_{0.5}N_{0.5}$ in inductively coupled plasma NF_3/O_2 and NF_3/Ar discharges has been performed. The etch rates in both chemistries increased monotonically with NF_3 percentage and rf chuck power. The rates were strong functions of plasma composition, ion energy and ion fluxes; and were independent of conductivity type for SiC. They went through a maximum with increasing ICP source power, which is explained by a trade-off between the increasing ion flux and the decreasing ion energy. The anisotropy of the etched features is also a function of ion flux, ion energy and atomic fluorine neutral concentration. Indium-tin-oxide (ITO) masks display relatively good etch selectivity over SiC (maximum of ~70:1), while photoresist etches more rapidly than SiC. The surface roughness of SiC is essentially independent of plasma composition for NF_3/O_2 discharges, while extensive surface degradation occurs for SiCN under high NF_3: O_2 conditions.

CHAPTER 1
INTRODUCTION

New interest in the design of magnetic sensors, magnetic memories, and other devices based on magnetic and magneto-resistive materials has been initiated by the discovery of multilayered "giant magnetoresistive"(GMR) materials[1] and more recently by the study of La-manganite perovskite "colossal magnetoresistive"(CMR) materials.[2] In both cases the implementation of practical devices requires the development and control of etching and patterning procedures which do not degrade the magnetic properties of the materials. Generally, the magnetic field response of magnetic thin-film materials is highly sensitive to their microstructural and interfacial properties. In the case of La-manganite materials, another limitation at present is that the observed field-induced resistivity transition is most sensitive above magnetic fields of about 1 Tesla. Thus the necessary bias field is too large to be produced by an electrical current within the device, as is done for typical low-field magnetoresistive sensors. Consequently it may be necessary to provide a fixed, built-in bias field within the device, from a hard magnet materials such as SmCo. In that case etch and patterning recipes must also be developed for such materials.

There has also been a revival of interest in Silicon carbide (SiC) based semiconductor electronic devices and circuits for use in high-temperature(> 250°C), high-power conditions under which conventional semiconductors cannot adequately

perform.[3-22] The applications range from greatly improved high-voltage switching[23-25] for energy savings in public electric power distribution and electric vehicles, more powerful microwave electronics for radar and communication[26] to sensors and controls for cleaner-burning more fuel-efficient jet aircraft and automobile engines.[27,28] SiC is the most mature of the candidate semiconductors, which include diamond and GaN, and has the advantage of high thermal conductivity and availability in both bulk, single-crystal and thin-film form. The two most common polytypes are 6H and 4H, although cubic material (3C) is also available[5,9,12,22]. There are a wide variety of device structures that have been fabricated in 6H, including thyristors, static induction transistors, Schottky diodes, metal-semiconductor field effect transistors (MESFETS) and various vertical Metal-Oxide-Semiconductor (MOS) devices.[3-22] There is also interest in SiCN alloys for heterostructure electronic devices. In all of these materials there is a need for pattern transfer capability.

CHAPTER 2
DRY ETCHING TECHNIQUES

2.1. The Transition from Wet to Dry Etching

Etch processes are judged by their rate, selectivity, uniformity, directionality (isotropy or anistropy), surface quality, and reproducibility. There are two different etching methods by using two quite different media: liquid chemicals (wet etching) and reactive gas plasmas (dry etching). Wet etching is performed by immersing the wafers in an appropriate solution or by spraying the wafer with the etchant solution.[29]Prior to the 1970s, virtually all semiconductor devices were etched in wet-etchant baths that were manually controlled.[30] Wet etching has some advantages: simple, low cost, low damage to the wafer, high selectivity and high throughput. However, as the requirements developed for increasing circuit density and narrower line-width in the manufacture of VLSI (very large- scale integrated circuit)/ULSI (ultra large- scale integrated circuit) devices, it became necessary to have new etching methods to replace the wet etching. The main limitations of wet etching include its isotropic nature, making it incapable of patterning sub-micron features, and the need for disposal of large amounts of corrosive and toxic materials. Dry etching methods became the favored approach for the etching processes for integrated circuit manufacture in the late 1960s and early 1970s.[31]These use plasma-driven chemical reactions and /or energetic ion beams to remove materials. The most significant advantage of dry over wet etching is that it provides higher resolution potential by overcoming the problem of isotropy.

Other benefits are the reduced chemical hazard and waste treatment problems, and the ease of process automation and tool clustering.

2.2. Mechanism of Dry Etching

As mentioned before, the predominant advantage of dry over wet etching is anisotropy. It is necessary to understand the range of directionality that may be obtained using dry etching techniques. Figure 2-1 indicates a comparison among isotropic, moderately anisotropic, and highly anisotropic processes.[32]

There are four basic categories for the mechanisms shown in Figure 2-2:[31]

a) Sputtering.

The interaction is purely physical, involving momentum transfer. The positive ions strike the substrate with high energy. The surface atoms receive the energy transferred from the ions and are ejected from the surface, leading to material removal. Sputtering lacks selectivity among different materials because the ion energy required to eject the surface atoms is very large compared with the differences in surface bond energies and chemical reactivity. Additionally, the etch rates are very slow by sputter etching.

b) Purely chemical.

The thermalized neutral radicals react with substrate material and create volatile products which will escape from the surface and be pumped out of the chamber. Purely chemical is the most selective mechanism. However it is usually non-directional (isotropy), and cannot maintain the small dimensions needed in the manufacturing processes.

c) Ion-enhanced energetic mechanism.

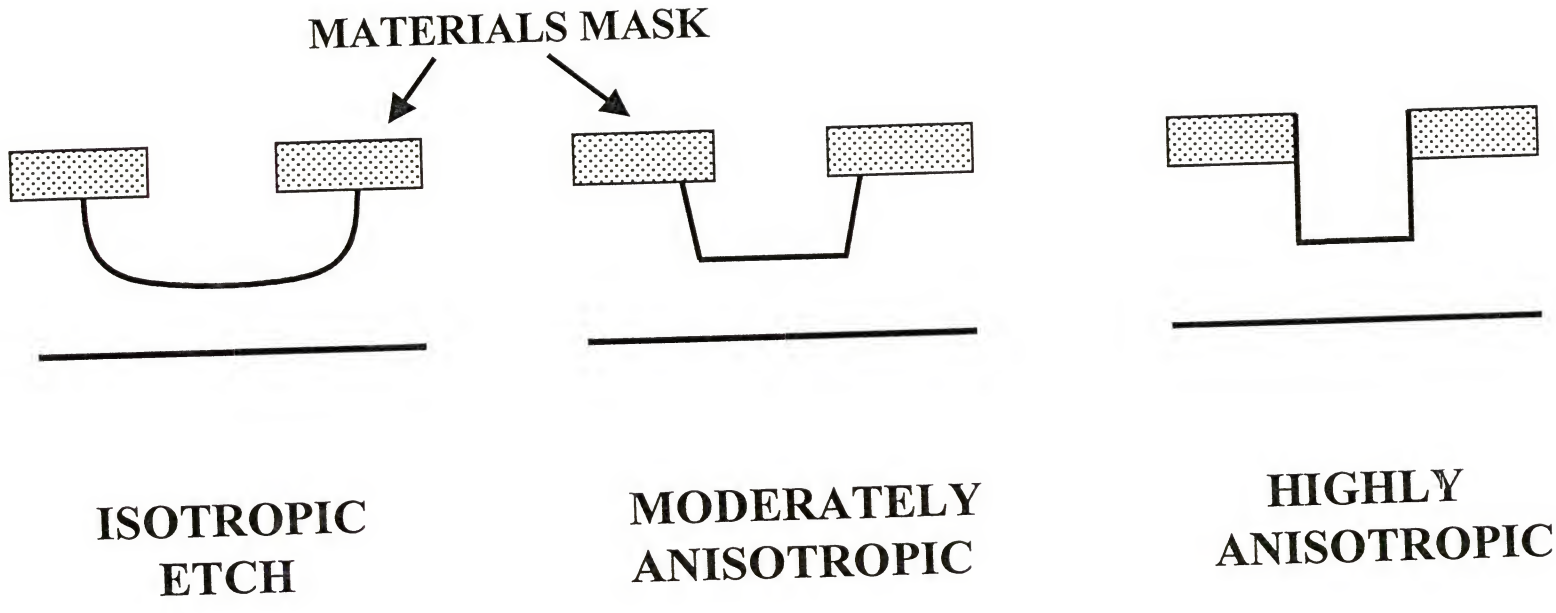

Figure 2-1 A comparison of isotropic (left), moderately anisotropic (middle), and highly anisotropic (right) etch processes.

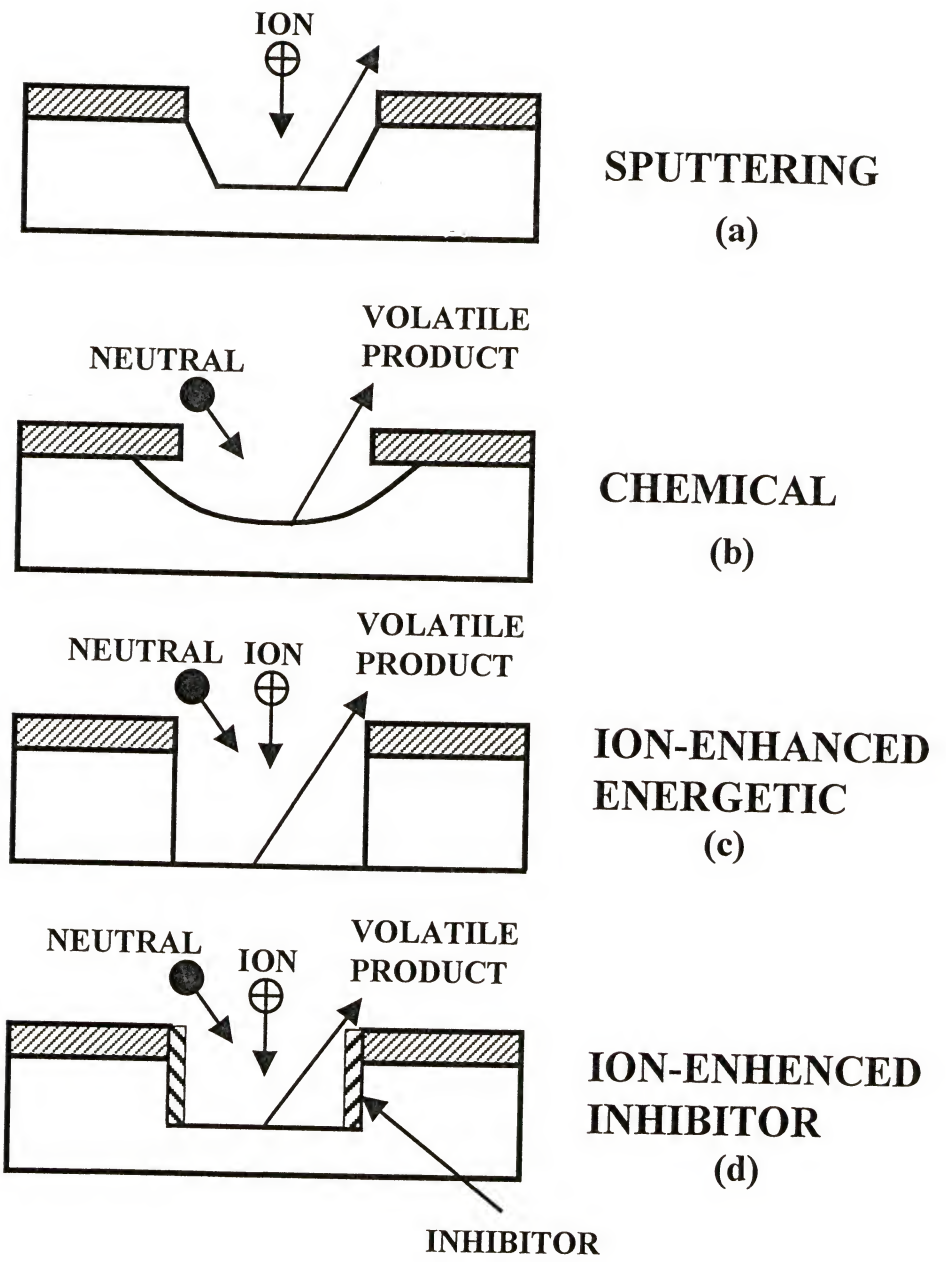

Figure 2-2 The four basic mechanisms of plasma etching:
(a) sputtering
(b) purely chemical
(c) ion-enhanced energetic mechanisms
(d) ion-enhanced inhibitor

There is little surface reaction with neutral radicals, until energetic ions enhance the reactivity of a substrate or product layer, allowing formation of the volatile product. Its particular advantage is anisotropy.

d) Ion-enhanced inhibitor.

The inhibitor species form a polymer-like material on the sidewall which helps to block etching of the sidewall and leads to increased anisotropy. The vertical sidewall of features are protected by the materials formed on the sidewall, while ion bombardment suppresses inhibitor growth on the horizontal surfaces that are etched. This phenomenon is called sidewall passivation.

2.3. Dry Etching Techniques

Dry etching takes place through a combination of chemical and physical components in order to obtain the desired results. The chemical etch component is rapid but isotropic, the physical component is slow but anisotropic. Therefore, we need to find the best etching technique in which the physical and chemical components are balanced.

Below are some of the dry etching techniques in common usage.[32]

1) Ion milling.

It is also called ion etching and is a purely physical process. A typical configuration of an ion milling machine employs a high energetic (500-800 eV) inert ion beam (typically Ar^+) to erode the surface by bombardment at the pressure $< 10^{-4}$ Torr (Figure 2-3).[33] The advantage of the technique is the complete absence of undercutting. The bad side is that there is little selectivity to mask materials, low etch rates, redeposited, ion on feature sidewalls and damage to the device due to the high ion energy.

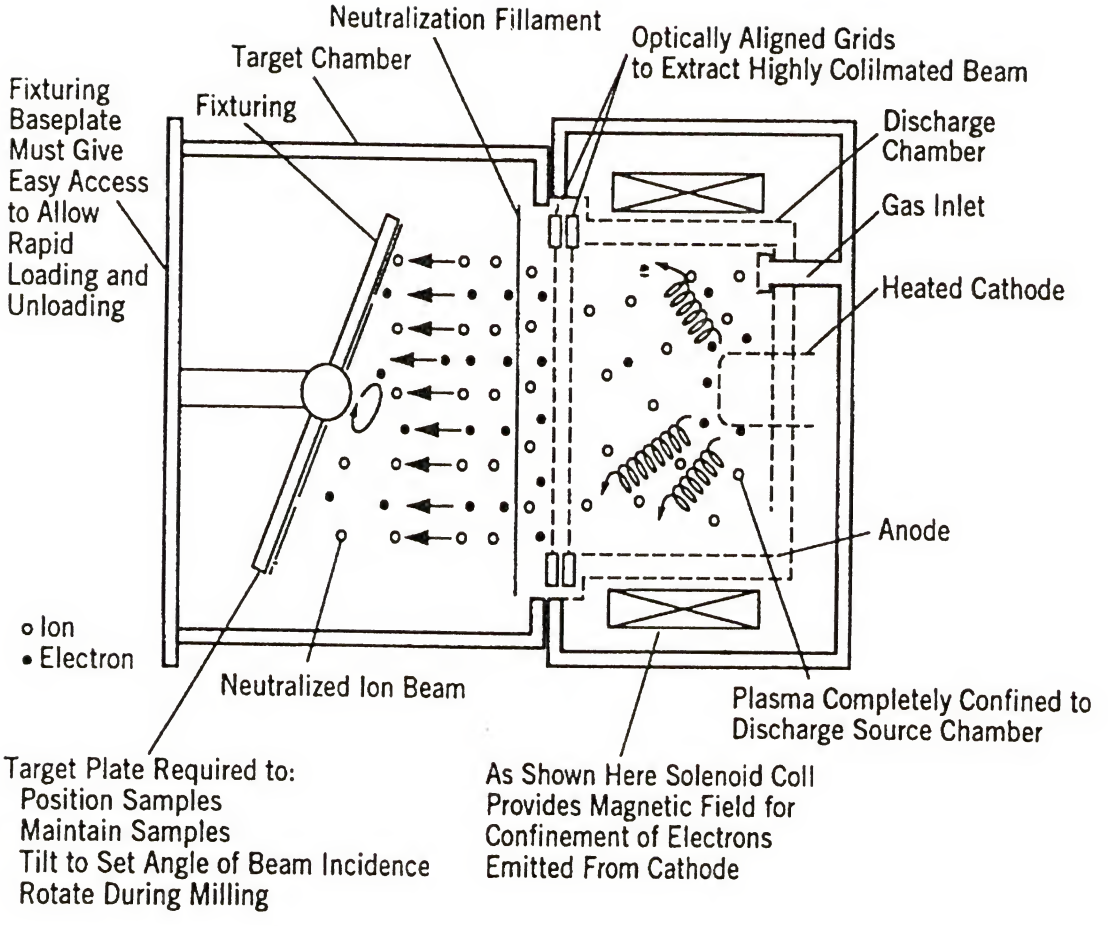

Figure 2-3 General configuration of an ion milling system.

2) Plasma etching.

A plasma is a gas which contains equal numbers of positive and negative charges, as well as neutral atoms, radicals, and molecules. These reactive species serve to chemically etch away materials such as resist, dielectrics, or metals at pressures >100mTorr. During the purely chemical etching process, three steps occur: adsorption of the necessary species on the materials surface, chemical reaction, and desorption of the products. The advantage of the technique is rapid etch rates, but the drawbacks are isotropy, a tendency for strong loading effects, and release of heat. Figure 2-4 shows the basic configuration of a parallel plate, planar plasma etching system. As noted there, there is a zone, referred to as the plasma sheath that separates the plasma from the sample electrode. The electrodes become negatively charged by the electrons from the plasma because the electrons have greater mobility than do positive ions in the plasma.

3) Reactive ion etching (RIE).

The mechanism of this technique is very similar to the plasma etching technique. To increase etch directionality, lower pressure and a different equipment configuration are employed. It is typically performed at 10-100mTorr pressure in an asymmetric parallel-plate reactor and is highly anisotropic which means the vertical etch rate far exceeds the lateral etch rate. As shown in Figure 2-5, the area of a flat electrode held the wafers is much smaller than the other electrode. The smaller electrode is powered by rf power (radiofrequency, usually 13.56MHz). The ion density is in the range 10^{10}-10^{11} cm^{-3} for most conventional rf discharges, and up to

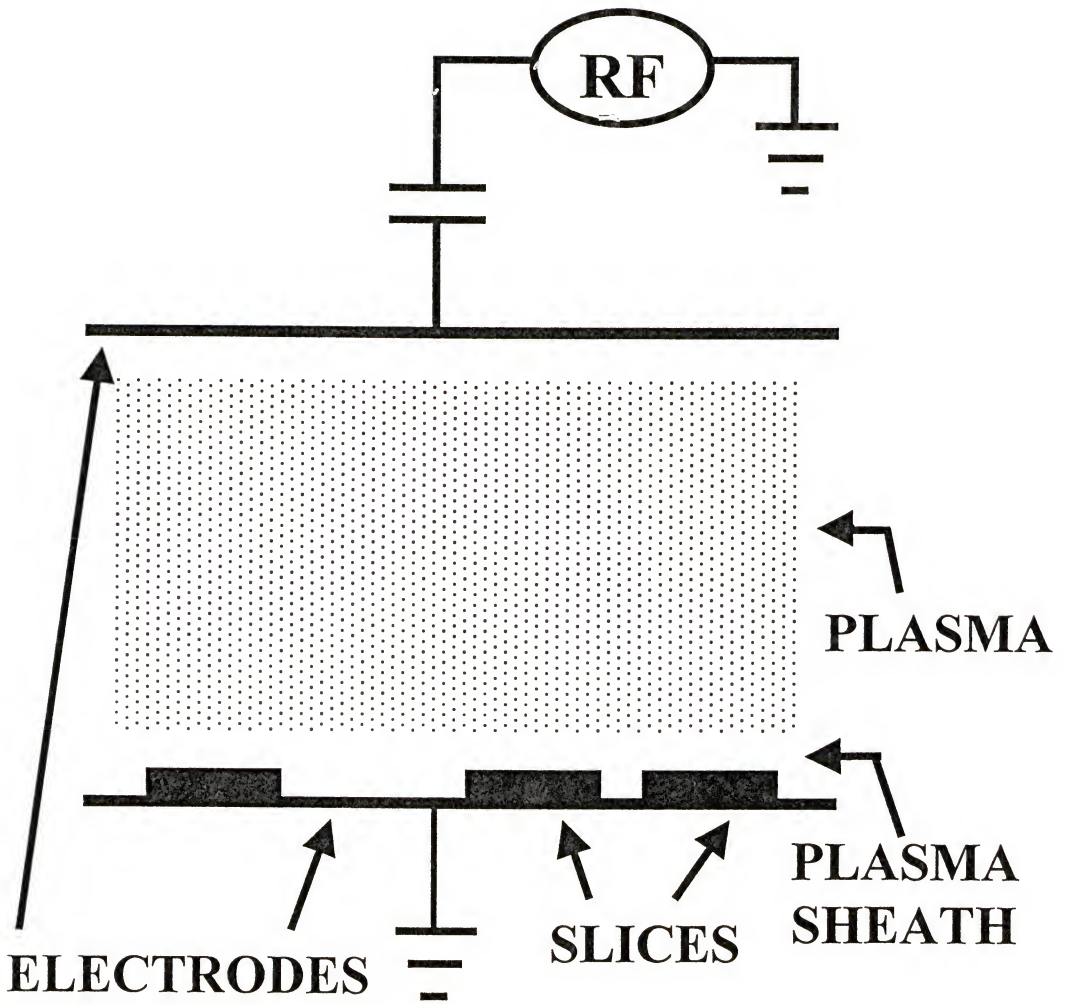

Figure 2-4 Configuration of parallel plate, planar plasma etching system.

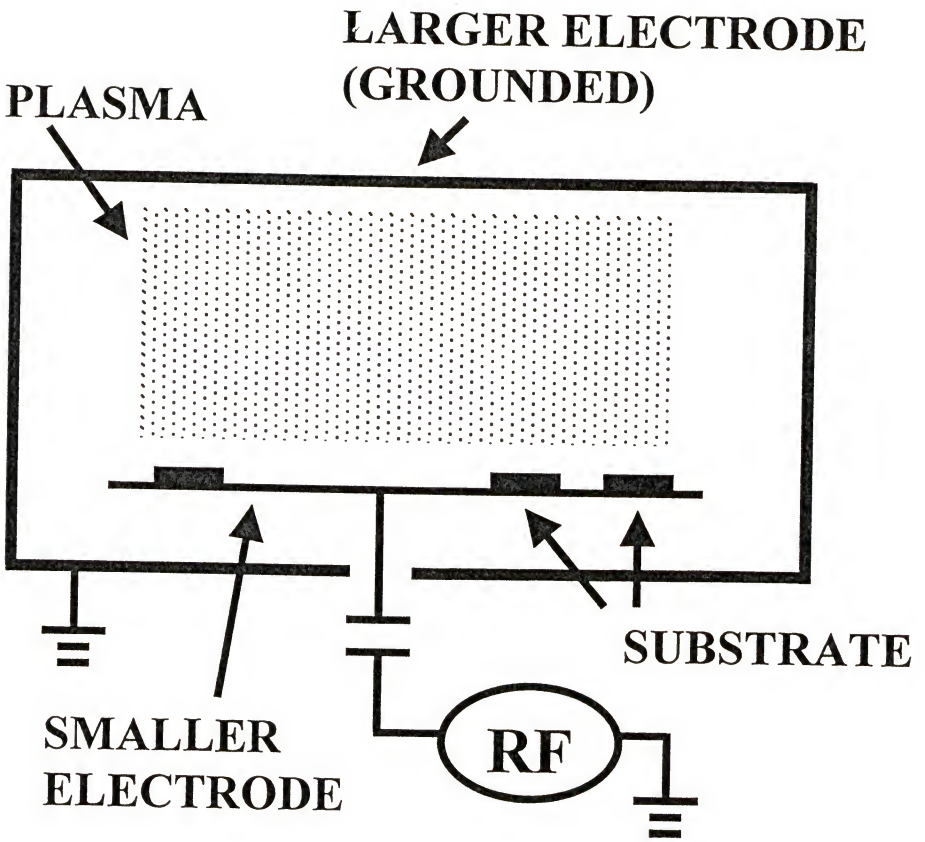

Figure 2-5 General configuration of a reactive ion etching (RIE) system.

10^{12} cm^{-3} for some of the new high-density discharge, such as Electron Cyclotron Resonance (ECR). The disadvantage of RIE is convective heating and is reduced by putting the wafers on a cooled stage to restrict temperature rise during etching.

4) Reactive ion beam etching (RIBE).

It is a further extension of RIE and could be considered an intermediate step between RIE and ion milling. Unlike RIE, some physical sputtering can remove the non-volatile products resulting from the chemical reactions. Pressure is usually in the range of 10^{-4} Torr. Compared to ion milling, RIBE has faster etch rates, better selectivity and fewer redeposition problems. However, compared with RIE and plasma etching, its throughput is lower. A typical RIBE system is shown in Figure 2-6.[33]

Table 2-1 lists the different characteristics for the different dry techniques.

Two particularly useful high ion density reactors are described below.

a) Electron Cyclotron Resonance (ECR).

A typical ECR reactor is shown schematically in Figure 2-7.[34] For a microwave frequency of 2.45 GHz (a frequency in common use for many applications), electron cyclotron resonance occurs at a magnetic field of 875 Gauss. The very energetic electrons efficiently ionize the gas species creating a plasma which contains ions and neutrals. Ion energy is controlled by separately biasing the sample position.

The ECR reactor has some advantages over the other plasma processing tools. First, it produces highly anisotropic etching for the lower neutral gas pressures, typically 0.2-10 mTorr, compared to 10-100 mTorr for RIE tools. Low operating pressure reduces ion collisionality in the substrate sheaths which is necessary for anisotropic etching of

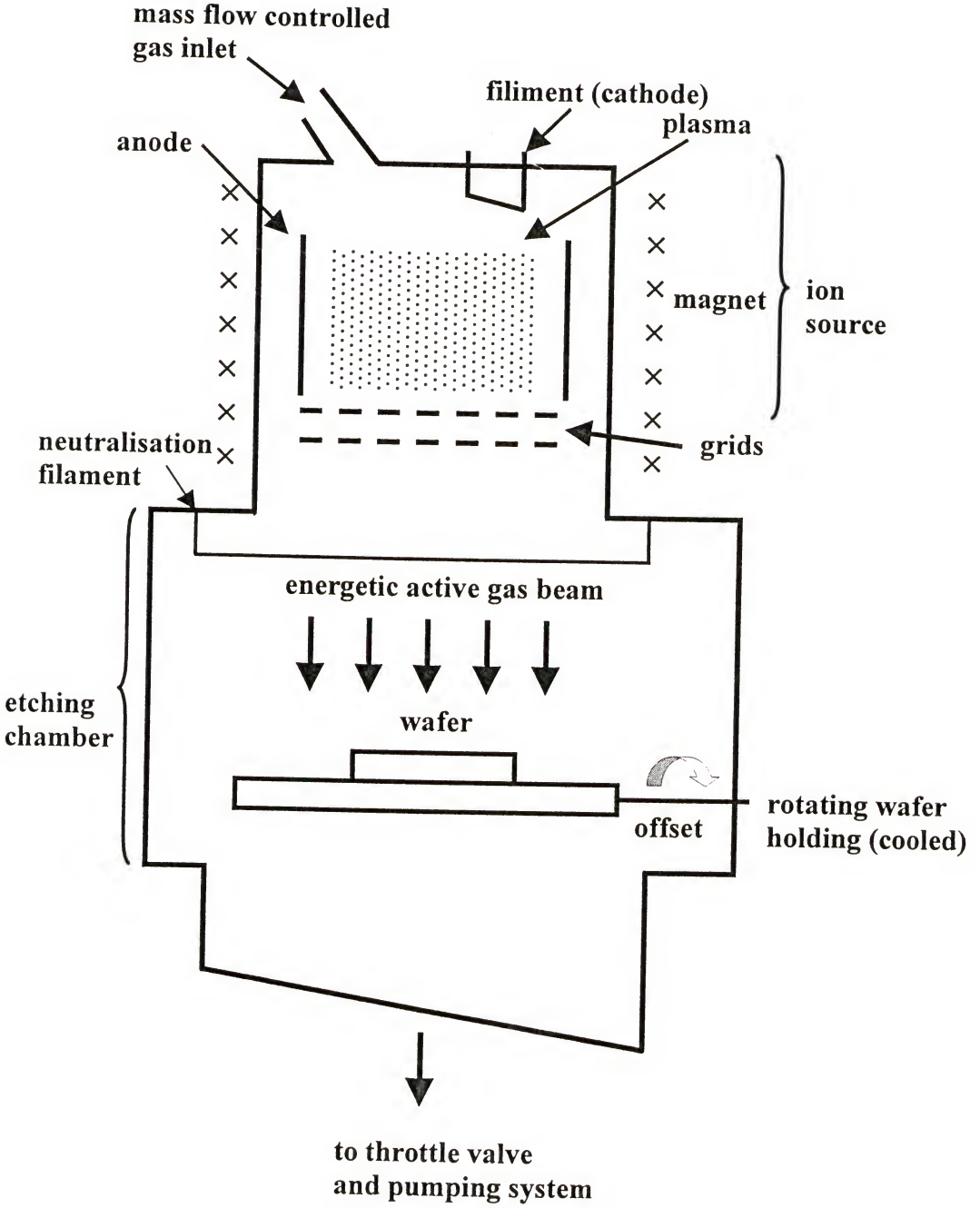

Figure 2-6 Typical reactive ion beam etching (RIBE) system using a broad beam ion source.

Table 2-1 Characteristics of the different dry etching techniques.

Characteristic	Ion Milling	Plasma Etching	RIE	RIBE
Mechanism	Physical	Chemical	Kinetically-Assisted Chemical	Kinetically-Assisted Chemical/ Physical
Directionality	anisotropic	isotropic	anisotropic	anisotropic
Pressure (Torr)	$< 10^{-4}$	0.1 - 5	0.01 - 0.1	10^{-4}
Equipment Configuration	Ion beam Accelerator	Barrel/Planar $A_s = A_o$	Planar $A_s < A_o$	Planar

A_s = Area of Electrode Holding Slices (Wafers).
A_o = Area of Other Electrode.

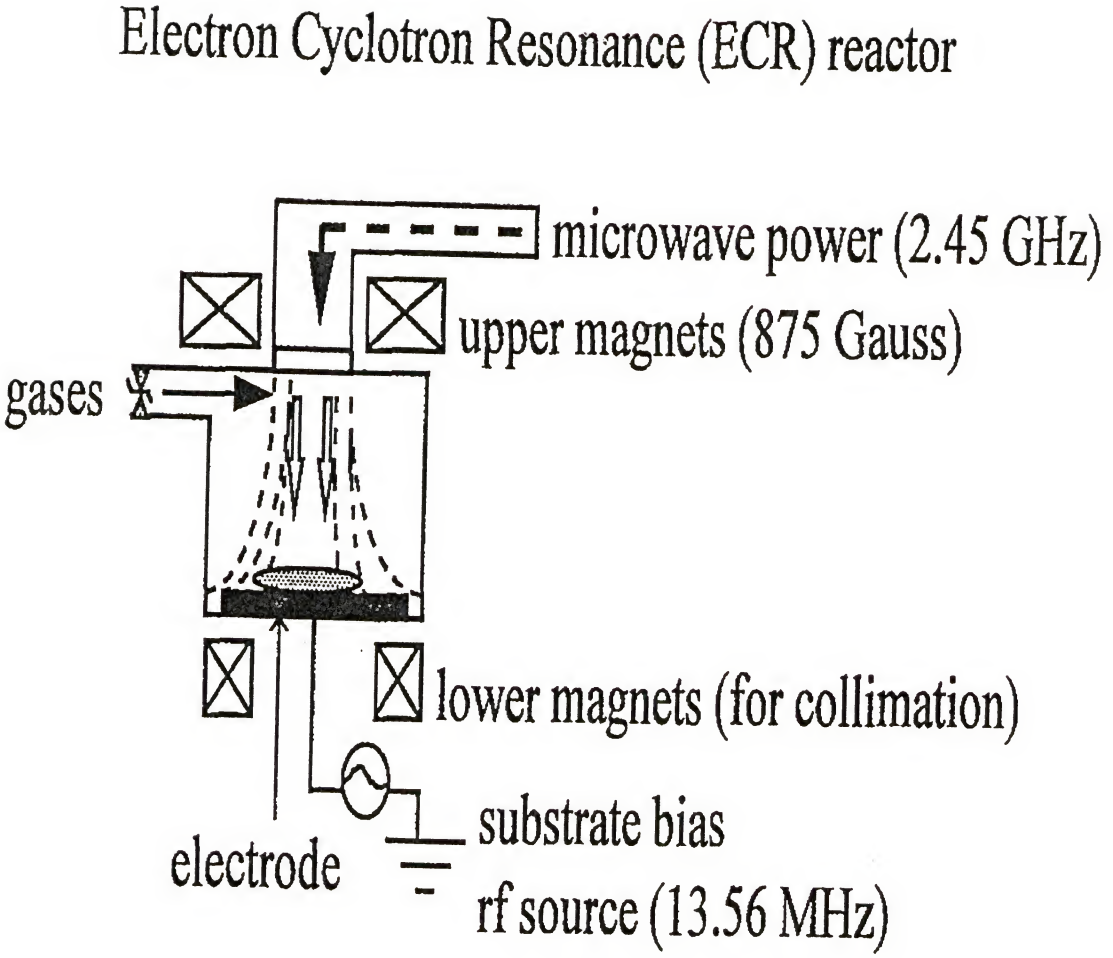

Figure 2-7 Schematic of ECR plasma etching system.

the smaller and increasingly high aspect ratio features in modern integrated circuits. Second, the etch rates are faster than with the RIE tools. The higher ion density (up to 10^{12} cm^{-3}, 10-100 times higher than the RIE tools) in the ECR reactor system implies higher ion-flux-driven processing rates which is important due to the high ownership costs of semiconductor processing tools. Third, we expect that there would be less substrate damage, due to the lower ion energies. Fourth, this tool can increase the etching selectivity between two substrate materials because of the low plasma potential, typically 15-30 eV without substrate biasing. Low plasma potential reduces the physical aspect of etching relative to the chemical and the physical damage to the substrate from high energy ion bombardment. Fifth, it can provide independent control of the ion energy and ion flux. Ion flux is controlled by varying the microwave power and neutral gas pressure, meanwhile, ion energy is controlled by changing the rf or DC biasing of the substrate holder.[35]

There are disadvantages as well as advantages. First, it is more expensive. Second, additional heat transfer mechanisms should be supplied such as He-backside cooling, since energetic ion bombardment of the wafer raises its temperature while the substrate is biased and the low pressure gas is a poor heat conductor. Third, the uniformity is not good due to the presence of the magnetic field which limits cross field diffusion of the plasma.[36]

b) Inductively Coupled Plasma (ICP).

A schematic of a typical ICP reactor is shown in Figure 2-8. Inside the shield is an rf coil. The important features of the coil are that it carries rf current and generates an rf field that is rotationally symmetric. The plasma is contained in the electrostatic shield

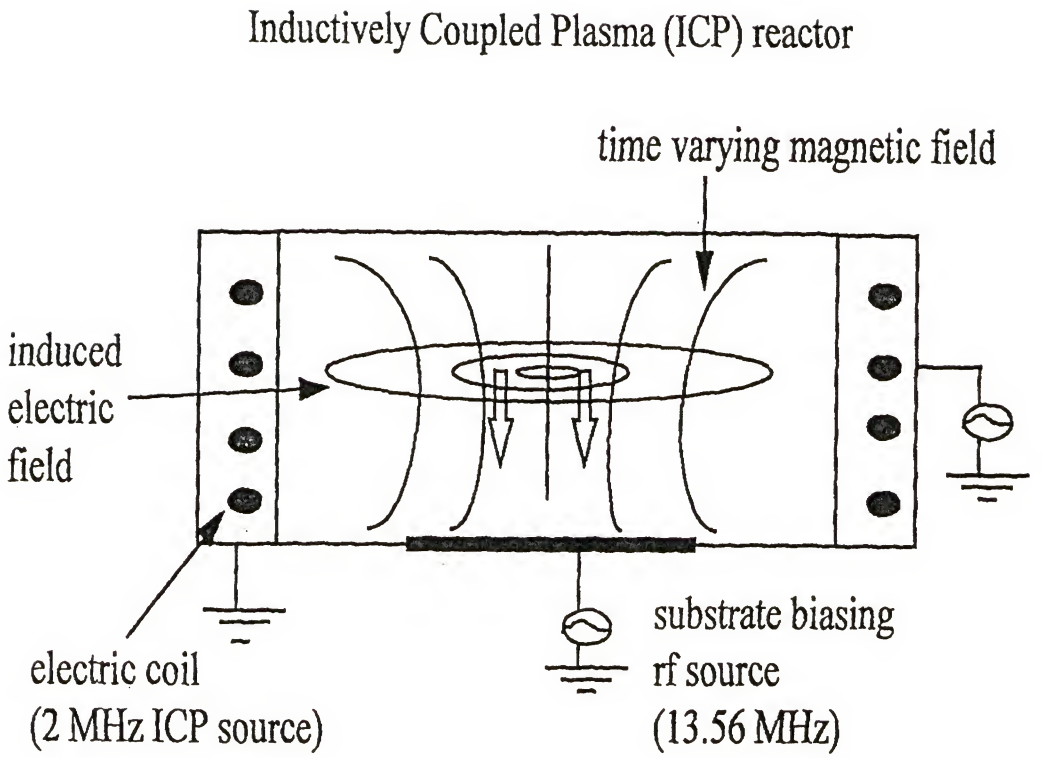

Figure 2-8 Schematic of Inductively Coupled Plasma (ICP) reactor.

or dielectric vacuum wall. The rf energy is confined to interact with the surface of the plasma in the same way that the rf currents act on any conductor. This is usually referred to as the skin effect which is the depth into the conductor materials that the rf field current will penetrate or flow. Plasma is presented only where there is an rf electrical field caused by the time rate of change of the magnetic field.[34]

The ICP system has advantages such as highly anisotropic etching due to the low pressure, high etch rates due to the high ion density, good selectivity, and independent control of the ion flux and ion energy (ion flux is controlled by the ICP source power and the gas pressure while ion energy is controlled by the rf or DC biasing of the substrate holder). Compared with the ECR reactor, the ICP system has more advantages when they are operated at the same low pressure (1 mTorr). First, the ICP reactor doesn't have the magnetic field. Second, larger size wafers can be processed in the ICP system. However, the additional heat transfer supplies such as He-backside cooling should be used as in the ECR reactor in order to reduce the temperature of the wafer due to the energetic ion bombardment while the substrate is biased.

CHAPTER 3
ETCHING $LaCaMnO_3$ AND SmCo

3.1. Materials and Methods

Thin films of $La_xCa_{1-x}MnO_3$ with x = 0.41 were prepared on MgO (001) and Al_2O_3(0001) single crystal substrates by liquid delivery metal-organic chemical vapor deposition (LD-MOCVD) as follows. An NZ-Applied Technologies liquid delivery vaporization system was used to deliver the 2,2,6,6-tetramethyl-3,5-heptanedionato (TMHD) organometallic precursors; $La(TMHD)_3$, $Sr(TMHD)_2$, $Mn(TMHD)_3$ and $Ca(TMHD)_2$ which were dissolved in 25 ml of freshly distilled solvent (diglyme) and vaporized (T = 250°C) at a rate of 1.66 μL/min. The gaseous mixture was then introduced into an EMCORE reactor. Nitrogen (100 sccm) served as a carrier gas and Oxygen (600 sccm) and N_2O (500 sccm), introduced directly into the reaction chamber, served as oxidants. During the deposition the substrates were held at a temperature of 700 °C and the reactor pressure was maintained at 5 Torr. After deposition, the films were slowly cooled under reaction conditions until the susceptor temperature was below 100 °C when the substrates were removed from the susceptor. No post-annealing was performed on the films. The deposition rate was ~ 15 Å/min.

The SmCo-based films were directly crystallized by RF diode sputtering (100 mTorr Ar) onto moderately heated (375-425°C) polycrystalline aluminum oxide substrates. The samples had a nominal composition of Sm 13%, Co 58%, Fe 20%, Cu 7%, Zr 2% and

were directly crystallized upon deposition into the disordered TbCu7 type crystal structure. The remanent ratio out of plane to in-plane was 0.030-0.038, with intrinsic coercivity 6.51-6.71 kOe. Both samples had the crystallite c-axes randomly aligned onto the substrate plane.

Samples of $LaCaMnO_3$ and SmCo were masked with either photoresist, SiN_x or apiezon wax for etching experiments. The dry etching was performed either in a Plasma-Therm SLR 770 reactor with an ASTEX 4400 low-profile electron cyclotron resonance (ECR) source[37] or a Plasma-Therm 790 reactor (ICP) in which the plasma is generated by a 3-turn inductive coil operated with up to 1000W of 2MHz power. For the ECR system, the ECR cavity was formed with an upper magnet (170 A) and collimated with a lower magnet (40 A). The process pressure was held constant at 1.5mTorr. The rf power (13.56 MHz) varied between 50 and 350 W and the microwave power was held constant at 1000 W. The plasma chemistries used were 15 standard cubic centimeter per minute (sccm) Ar, 10 sccm SF_6/5 sccm Ar, 2.5 sccm CH_4/7.5 sccm H_2/5 sccm Ar or 10 sccm Cl_2/5 sccm Ar. For the inductively coupled plasma (ICP) system, the sample position was separately powered with 0-450W of 13.56MHz power and the chuck is He backside-cooled to hold the sample temperature to $\leq$ 40°C. Process pressure was held constant at 5mTorr for all experiments. The BI_3 (melting point 40°C) and BBr_3 (boiling point 91°C) were held at ~ 45°C within a stainless steel vacuum vessel- total gas loads of 10 sccm were injected into the ICP source through electronic mass flow controllers. The etch rates were determined by stylus profilometry measurements using a Dektak or Tencor system after the removal of the mask with acetone. Surface morphologies were examined with scanning electron microscopy (SEM) and atomic force microscope (AFM) using a Si tip

in tapping mode, while the near surface stoichiometry was obtained from auger electron spectroscopy (AES) experiments.

Table 3-1 lists boiling points of some potential etch products in the plasma chemistries investigated here.[38] To achieve smooth etched surfaces, it is obviously necessary to remove the etch products at equal rates for all of the elemental constituents. For BI_3 and BBr_3 discharges, the products for oxygen are considerably more volatile than for the other elements, which makes it difficult to achieve smooth etched surfaces. However the Cu and Mn products with both BI_3 and BBr_3 are somewhat more volatile than with the Cl_2 and F_2 chemistries.

3.2. Results and Discussion

Figure 3-1 shows the dependence of $LaCaMnO_3$ etch rate on dc self- bias on the sample chuck for the four different plasma chemistries. Note that the results for Cl_2/Ar basically follow those for pure sputtering (Ar), indicating that the La,Ca and Mn chlorines are not particularly volatile even at the high ion fluxes ($\sim 10^{15}$ ions$\cdot$cm^{-2} $\cdot$sec^{-1}) available in the ECR tool. In other words, the etching is limited by the sputter yield at each ion energy; to increase the volatility of the chloride etch products it would be necessary to increase the substrate temperature. This is generally not an attractive option from a practical viewpoint because of the limitation it places on mask materials and the requirement for reproducible thermal contact for each sample.[39,40] The results for the SF_6/Ar and CH_4/H_2/Ar plasma chemistries show that the etch products for these are even less volatile and the etching is most likely retarded by formation of a selvedge or reaction layer with these chemistries.

Table 3-1: Boiling Points of Potential Etch Products of $LaCaMnO_3$ and SmCo

Etch Products	Boiling Point (°C)	Etch Products	Boiling Point (°C)	Etch Products	Boiling Point (°C)
$LaCl_3$	>1000	Cl_2O	2.2	SmH_2	.....
LaF_3	.....	ClO_2	11	$(CH_3)_2Sm$	.....
La_2S_3	2100 vac.	Cl_2O_3	.....	$CoCl_2$	1049
LaI_3	>1000	Cl_2O_6	≈200	$CoCl_3$	.....
$LaBr_3 \cdot 7H_2O$	1577	O_2	-183	CoF_2	≈1400
$(CH_3)_3La$	.....	Cl_2O_7	82	CoF_3	.....
$CaCl_2$	1935.5	F_2O	-144.75	CoH_2	.....
CaF_2	2533.4	F_2O_2	-57	$(CH_3)_2Co$	.....
CaH_2	d 816	H_2O	100	$FeCl_3$	316
CaI_2	ca1100	$(CH_3)_2O$	-23.6	$FeCl_2$	1023
$CaBr_2$	806-812	BrO_2	9	FeF_3	726
$(CH_3)_2Ca$	.....	Br_2O	4.5	FeF_2	1837
CaS	d	Br_3O_8	.....	CuCl	1490
$MnCl_2$	1190	IO_2	13	CuF	s 1100
$MnCl_3$	d	I_2O_4	.....	$ZrCl_2$	d 350
MnF_2	> 856	I_2O_5	.....	$ZrCl_3$	s 331
MnF_3	d	I_4O_9	d75	ZrF_4	s 600
MnH_2	.....	$SmCl_2$	> 740	ZrH_2	.....
MnI_2	subl vac500	$SmCl_3$	.....	ZrS_2	>1550
$MnBr_2$	858	SmF_2	>2400		
$(CH_3)_2Mn$	.....	SmF_3	2323		

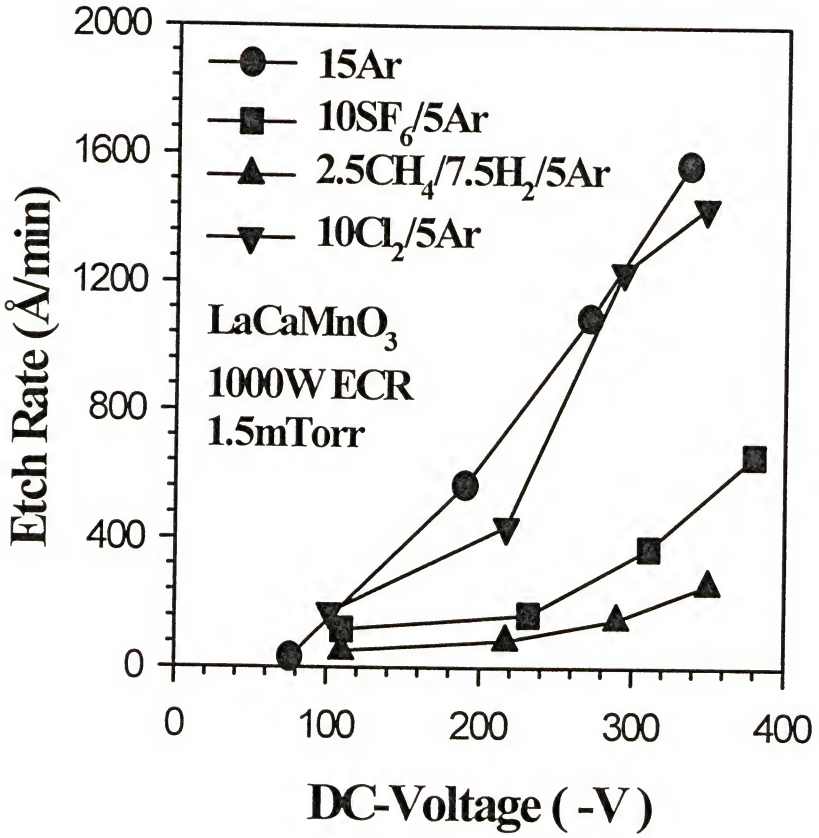

Figure 3-1 Etch rate of $LaCaMnO_3$ in various plasma chemistries as a function of chuck self-bias. The ECR source power was held constant at 1000W.

There was a substantial degree of chemical enhancement observed for the etching of SmCo in Cl_2/Ar chemistries, as shown in Figure 3-2. The etch rate is approximately a factor of 10 to 12 higher than for pure Ar up to dc self-biases of ~ -217V; at higher biases the etch rate with Cl_2/Ar saturates and then decreases. The self-bias corresponds fairly closely to the acceleration voltage experienced by ions impinging on the sample.[41] As this voltage increases so does the average ion energy. Up to a particular energy, the etch rate is increased by the higher sputtering efficiency that more effectively desorbs the etch products. However above this energy (in these experiments ~ 250eV) the ions are able to desorb the chlorine radicals before they are able to react with the SmCo and hence the etch rate decreases. The SF_6/Ar plasma chemistry provides etch rates faster than pure sputtering at biases up to ~ -200V, but show a dependence on bias that is less than that for Ar at higher values.

Since the etching for both $LaCaMnO_3$ and SmCo is a strong function of ion energy, we would expect a fairly anisotropic pattern transfer. Figure 3-3 shows SEM micrographs of features etched into both materials using a Cl_2/Ar plasma at -200V dc self-bias and an SiO_2 mask which was subsequently removed. The etched surfaces under these conditions are essentially as smooth as the unetched regions and the sidewalls are reasonably vertical. The striations on the sidewall are typically observed on dry etched features and originate from roughness on the edges of the original photoresist mask that was used to transfer the pattern into the SiO_2.[42,43]

Representative AFM scans from $LaCaMnO_3$ sample before and after etching are shown in Figure 3-4. Note that CH_4/H_2/Ar etching at relatively low biases does not produce much surface roughening (increase from 10.72 nm root-mean-square(RMS)

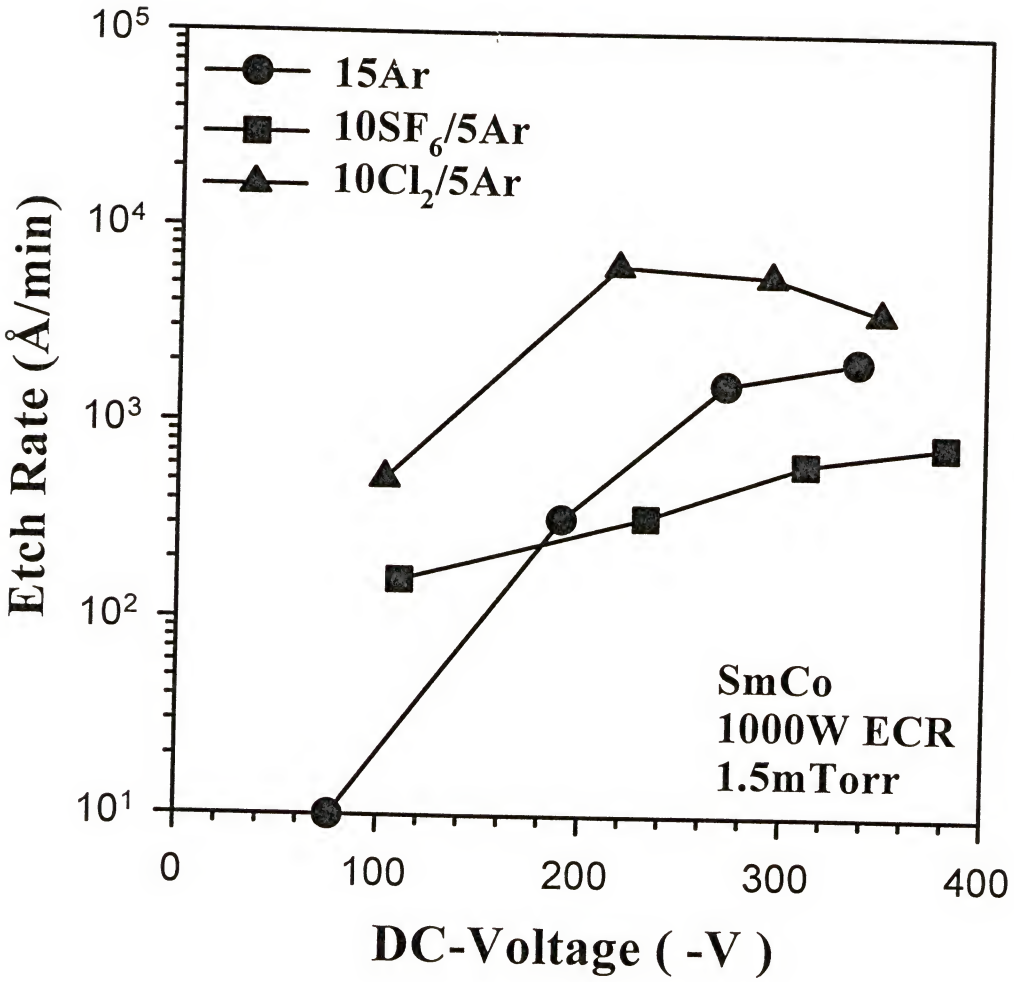

Figure 3-2 Etch rate of SmCo-based films in various plasma chemistries as a function of chuck self-bias. The ECR source power was held constant at 1000

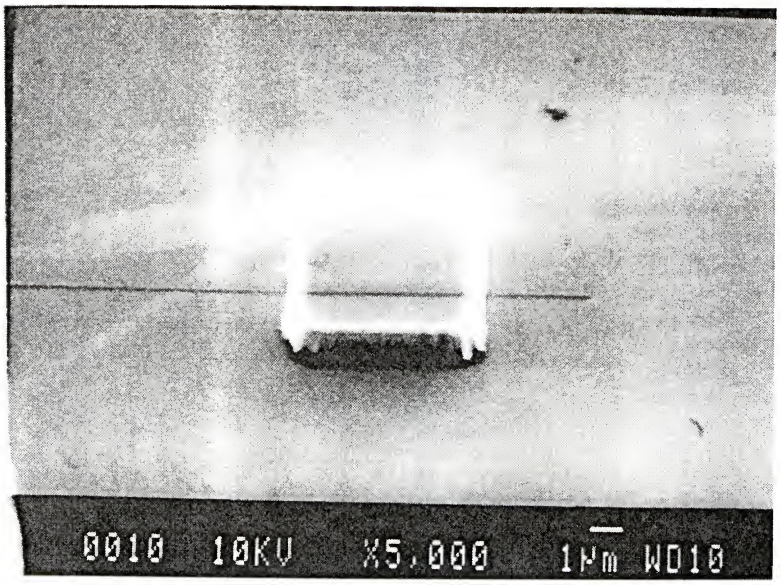

LaCaMnO $_3$/Al_2O_3 Cl_2/Ar ECR etch

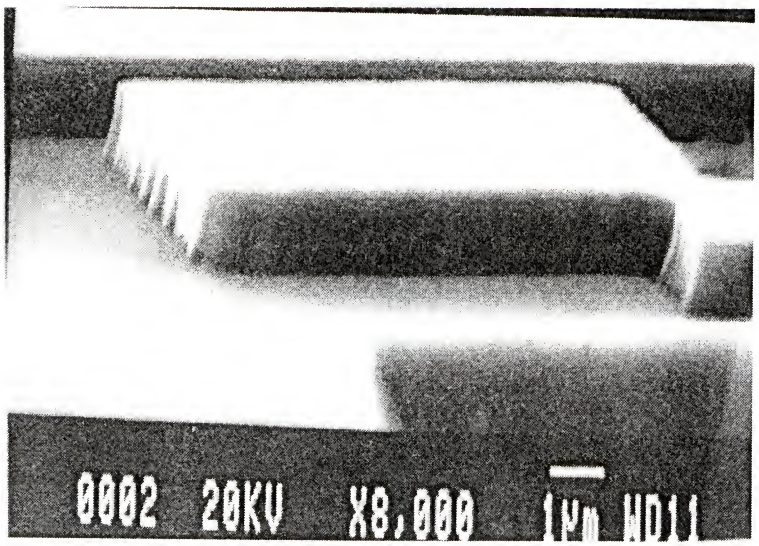

SmCo Cl_2/Ar ECR etch

Figure 3-3 SEM micrographs of features etched into $LaCaMnO_3$ (top) and SmCo-based films (bottom) using a Cl_2/Ar plasma. The SiO_2 masks have been removed.

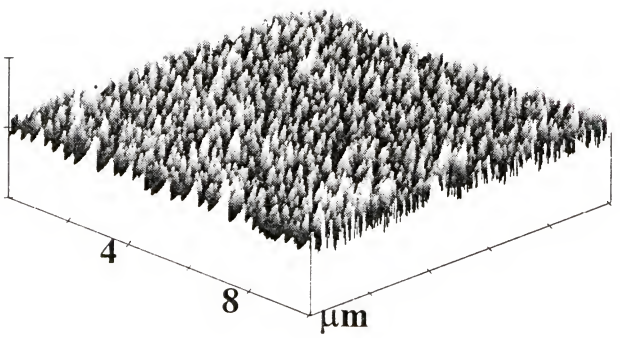

Control
RMS: 10.717 nm

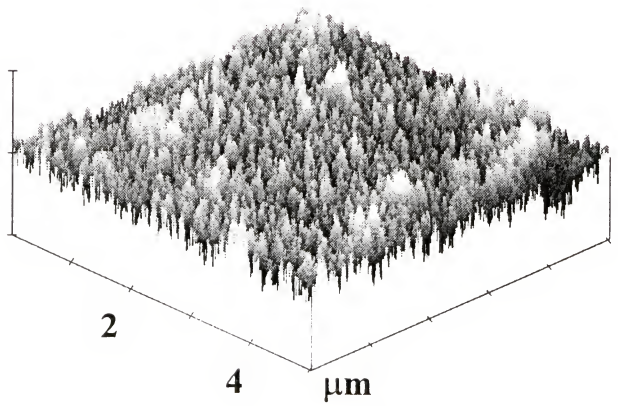

$2.5CH_4/7.5H_2/5Ar$
DC -217 V
RMS: 11.968 nm

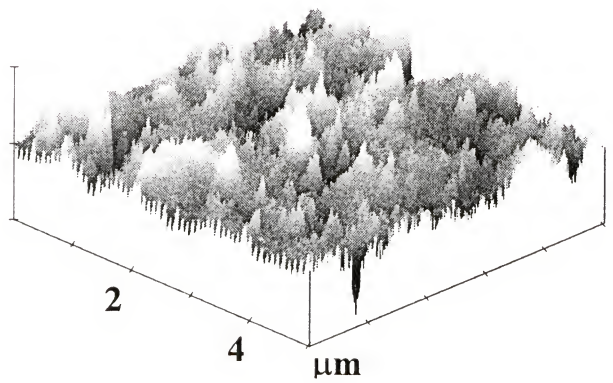

$10Cl_2/5Ar$
DC -293 V
RMS: 17.489 nm

Figure 3-4 AFM scans of $LaCaMnO_3$ before (top) and after etching in $CH_4/H_2/Ar$ (center) or Cl_2/Ar (bottom).

roughness on the control sample to 11.97 nm on the etched material). This is consistent with the SEM micrographs of the previous Figure. However it was typically observed that for higher dc self-biases, the surface morphology degraded. For example, the AFM scan at the bottom of Figure 3-4 shows that for a self-bias of -293V in a Cl_2/Ar discharge, the RMS roughness increased to 17.5 nm. This is a fairly typical trend in dry etching of complex materials containing elements with significant differences in mass number.[44-46] Under conditions where the etching is desorption- or sputter-limited, the lighter elements will tend to be preferentially sputtered, leaving the near-surface non-stoichiometric and rougher than that of a control sample.[47,48]

To better understand the role of plasma chemistry and ion energy in the surface roughening, AES surface scans and near-surface depth profiles were measured on the samples from Figure 3-4. The results from the control material are shown in Figure 3-5. The sputter rate during depth profiling was ~ 60Å·min^{-1}. The surface scan shows the lattice constituents, adventitious carbon and some Si contamination (which we observe on all samples we examine by AES, whether they be oxides, semiconductors or magnetic materials). Dry etching with the CH_4/H_2/Ar chemistry at moderate dc self-bias (-217 V) produced little change in the AES surface scan (Figure 3-6). By sharp contrast in the sample etched in Cl_2/Ar at higher bias (-293V), the near-surface is deficient in the lighter elements O, Ca and Mn (atomic weights of 16,40 and 55, respectively compared to 139 for La), as shown in Figure 3-7. The surface roughness also leads to non-abrupt depth profiles, which explains the prolonged Cl signal. The Cl originates from the presence of remnant etch products that were not completely desorbed because of their low volatility.

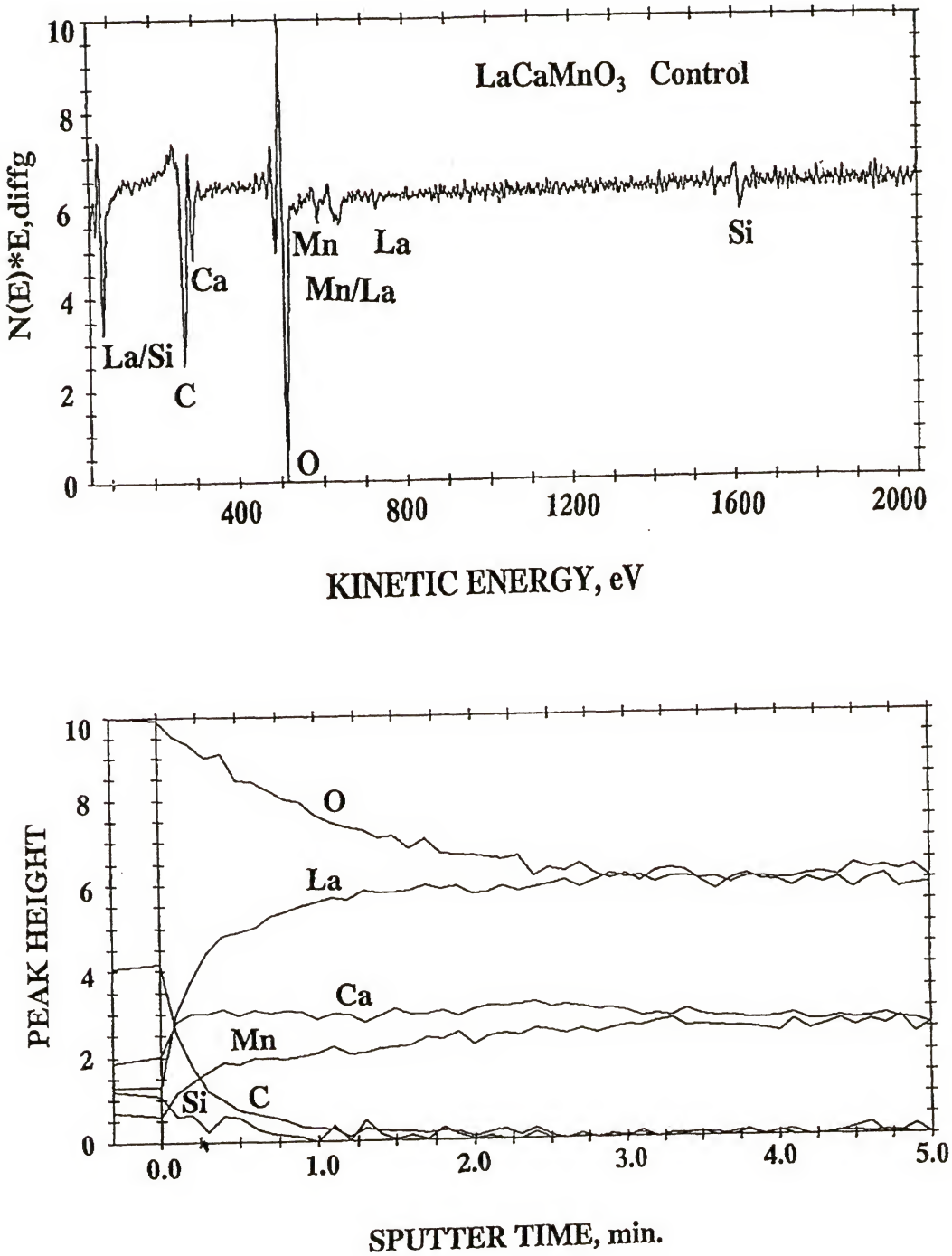

Figure 3-5 AES surface scan (top) and depth profile (bottom) from an unetched $LaCaMnO_3$ control sample.

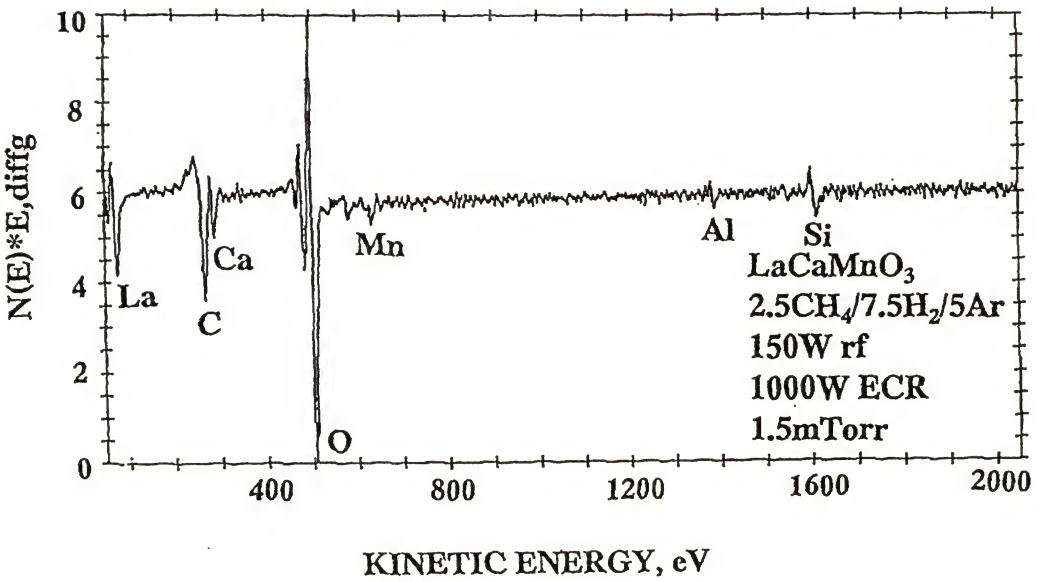

Figure 3-6 AES surface scan from $LaCaMnO_3$ after etching in a $CH_4/H_2/Ar$ ECR plasma.

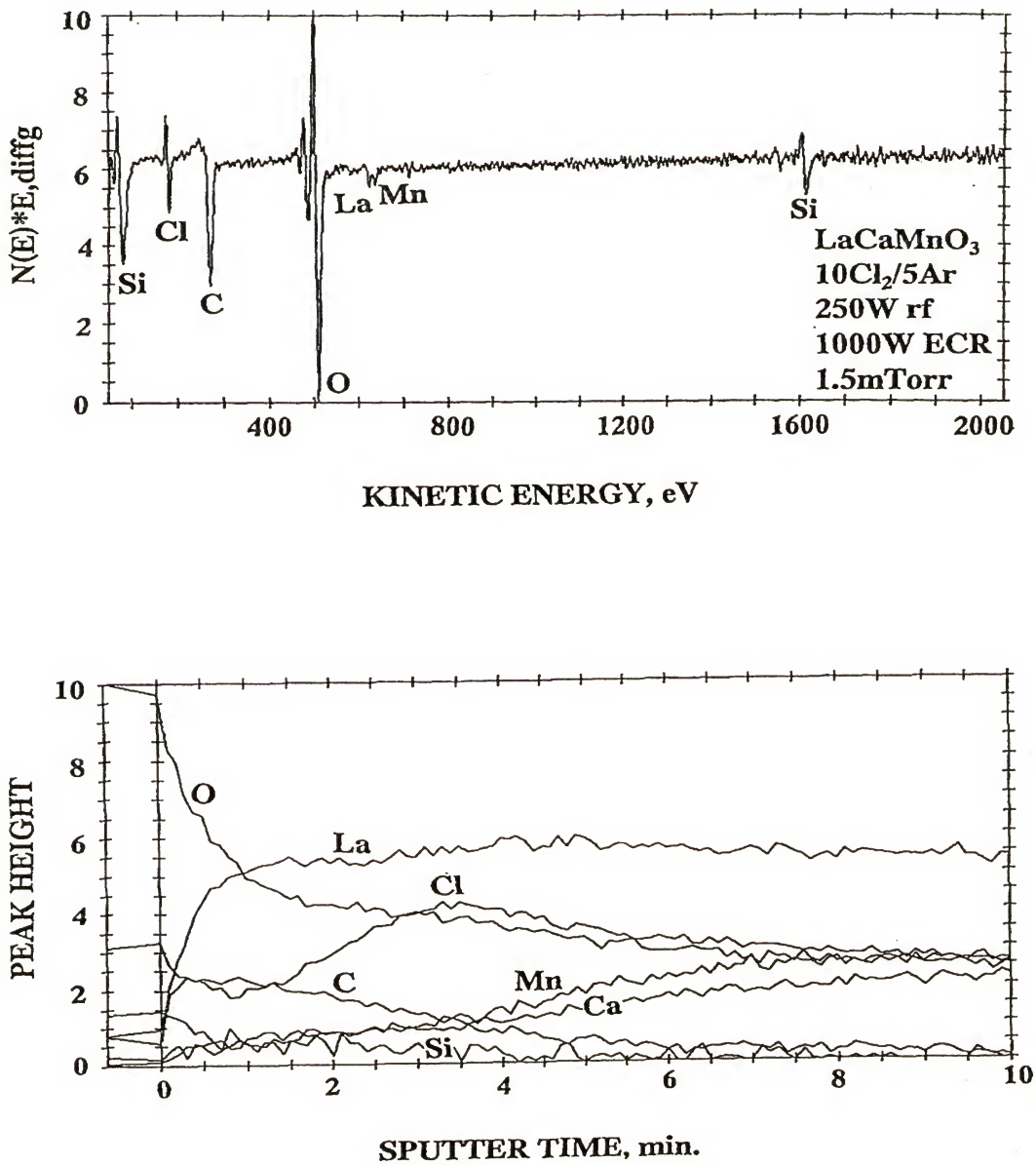

Figure 3-7 AES surface scan (top) and depth profile (bottom) from $LaCaMnO_3$ after etching in a Cl_2/Ar ECR plasma.

An additional important consideration is selection of a mask material for the etching process. Photoresist is typically not suitable for high density plasma processes because the high ion currents lead to reticulation and loss of dimensional stability.[49] Figure 3-8 shows Cl_2/Ar etch selectivity for both SmCo and $LaCaMnO_3$ over the dielectrics SiO_2 and SiN_x. The dielectrics were deposited by plasma-enhanced chemical vapor deposition at 250 °C using SiH_4/O_2 and SiH_4/NH_3, respectively. Since there is basically no chemical enhancement for etching $LaCaMnO_3$, there is also no selectivity over the dielectrics. This is a severe limitation if one needed to pattern deep features into $LaCaMnO_3$ because the mask thickness would need to be at least as thick as the required etch depth. For SmCo however, the etch selectivity is ~ 4 at low rf chuck powers and increases initially as this power is increased because the etch rate of the magnetic material rises faster than that of the dielectrics. At higher powers the selectivity decreases because of the fall-off in etch rate of the SmCo (Figure 3-2), and the fact that the dielectric etch rate continues to increase as ion energy is increased. Therefore, the modest chuck self-bias region is advantageous from the viewpoint of higher etch rates and selectivity with respect to the mask materials.

To investigate the potential impact of dry etching on SmCo films, magnetic hysteresis loops were obtained with the field applied both parallel and perpendicular to the film plane, before and after etching under various plasma conditions. The films investigated, with thickness of about 10 μm, displayed a range of coercive fields H_c (parallel) ≈ 3.3-9.8 kOe and H_c (perpendicular) ≈ 4.0-7.3 kOe, and were exposed for 1 minute to pure Argon plasmas with source powers up to 1500W and rf chuck powers up to 450W. Within our experimental error (±5%), no changes in magnetic properties were

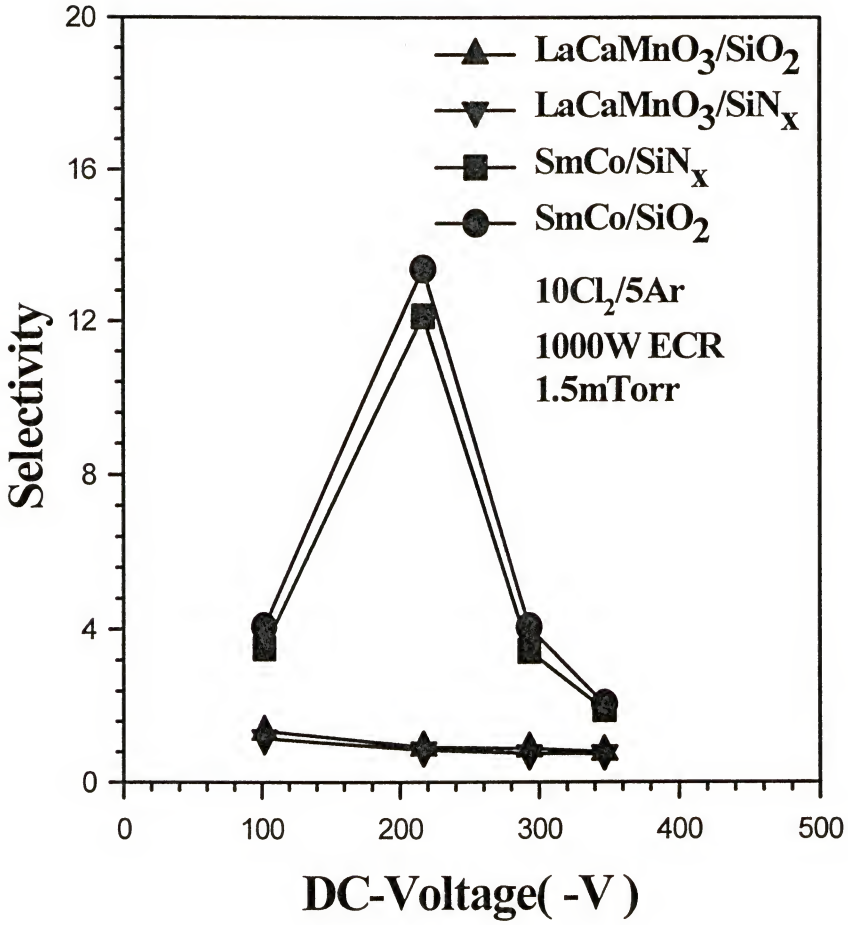

Figure 3-8 Selectivity for etching SmCo-based films or $LaCaMnO_3$ over either SiO_2 or SiN_x mask material, as a function of chuck self-bias.

detected after etching, indicating that there was no gross damage produced by the etch process.

We used two novel plasma chemistries, BI_3 and BBr_3, for dry etching of $LaCaMnO_3$ because there is no chemical enhancement in etch rate over simple sputtering for Cl_2, SF_6 or CH_4/H_2 plasma. We observed a small degree of chemical enhancement with both chemistries at low halide composition (20-40% by flow) in the discharge. The etching is still strongly dependent on ion energy and flux, and is highly anisotropic. Etch yields are typically low (<0.3) under inductively coupled plasma conditions.

Figure 3-9 shows the dependence of $LaCaMnO_3$ etch rate (top) on BI_3 or BBr_3 percentage in 750W source power, 350W rf chuck power halide/Ar discharges. For both chemistries the etch rate initially increases as halide is added, indicating the presence of some chemical enhancement in the etch mechanism, but beyond ~20% by flow the rate decreases forward the value obtained by pure Ar sputtering. The same trends are reflected in the etch yields (Figure 3-9, bottom) calculated from a simple model for ion current in this ICP tool.[50] Note that these yields are low, with up to 50 ions required to remove one atom of each of the lattice constituents. The fact that both etch rate and yield decrease at higher halide contents in the discharge is consistent with adsorbed iodine or bromine neutrals blocking the surface to ion-assisted desorption of the etch products, the same mechanism that limits NiFe etching in Cl_2/Ar discharges.[51] The important parameter is thus the ion-to-neutral ratio at the sample surface. If this is too high then there will be predominantly physical sputtering, and if it is too low a selvedge layer will form that retards etching.

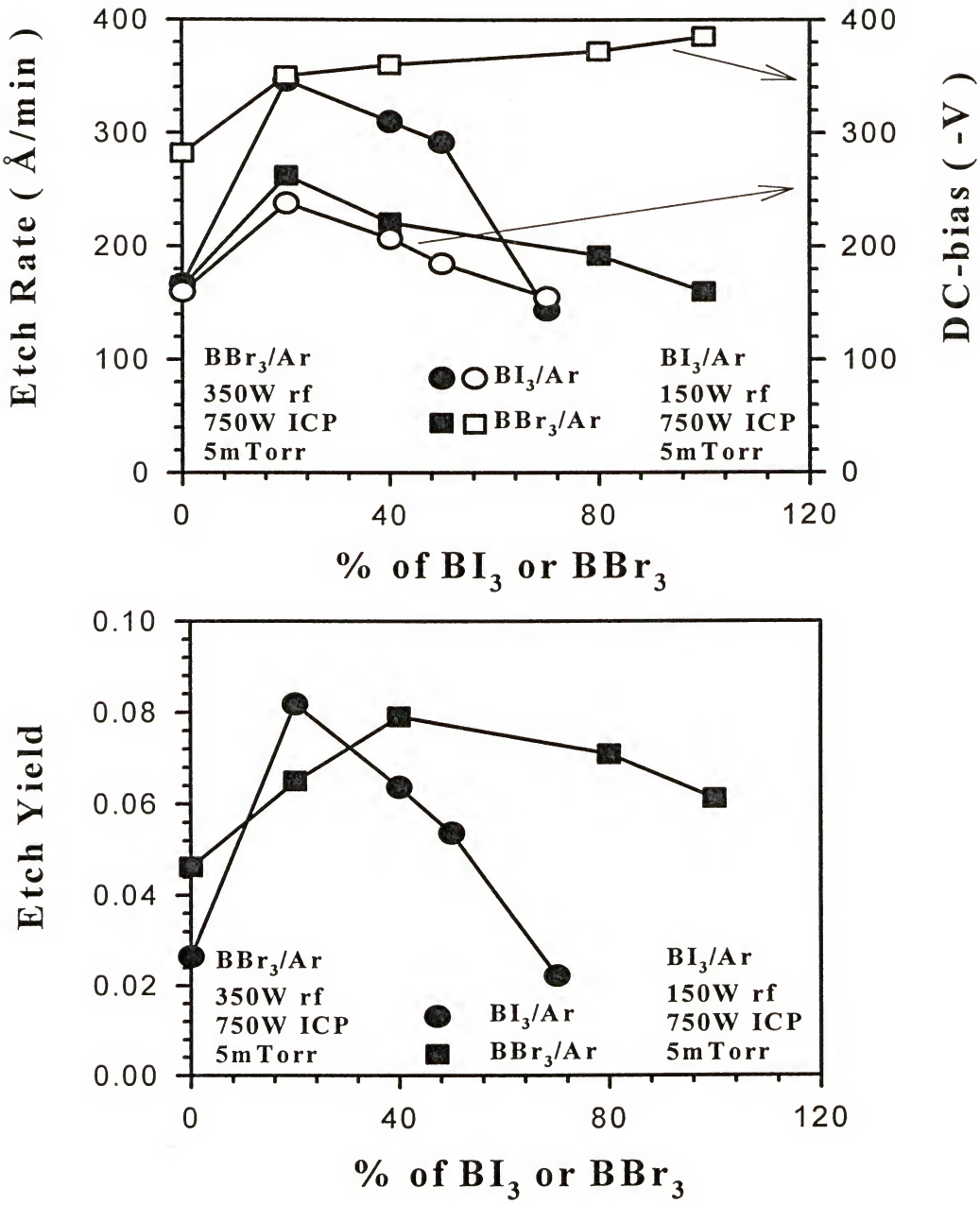

Figure 3-9 Etch rate (top) and etch yield (bottom) for $LaCaMnO_3$ in 750W ICP source power discharges of either BI_3/Ar or BBr_3/Ar, as a function of halide gas percentage. The rf chuck power was 150W for the BI_3/Ar and 350W for the BBr_3/Ar.

Since the etch products have generally low volatility, then one would expect the etch rate to be strongly dependent on ion energy. Figure 3-10 shows etch rate and yield as a function of the rf power and the associated induced dc chuck bias for a particular discharge composition. Note the rates increase montonically with rf power, consistent with a desorption-limited process, and also that BI_3 provides higher rates than BBr_3.

As mentioned above, ion flux is an important factor in the etch process. Figure 3-11 shows rate and yield data as a function of ICP source power for particular discharge compositions. While the etch rate continues to increase with this power due to the increasing ion flux and degree of plasma dissociation, the etch yield actually decreases under these conditions. This is consistent with the postulation that ion/neutral ratio is the key parameter controlling the efficiency of the etching.

The etched surface morphologies generally tended to improve slightly with increasing ion flux. Figure 3-12 shows AFM scans of samples etched in BI_3/Ar discharges at different source powers, while Figure 3-13 shows similar data for BBr_3/Ar. The root-mean-square (RMS) roughnesses obtained over 10×10 μm^2 areas are plotted in Figure 3-14. It is often observed that ion-driven etch processes will lead to some degree of surface smoothing on initially rough samples because of the angular dependence of ion mill rate removing sharper features more rapidly than flat regions. A competing mechanism is that ion energy decreases with increasing ICP source power, and this could produce less preferential sputtering of the lighter lattice elements. Our past data on dependence of surface morphology on ion energy suggests that both effects play a role in determining surface smoothness.

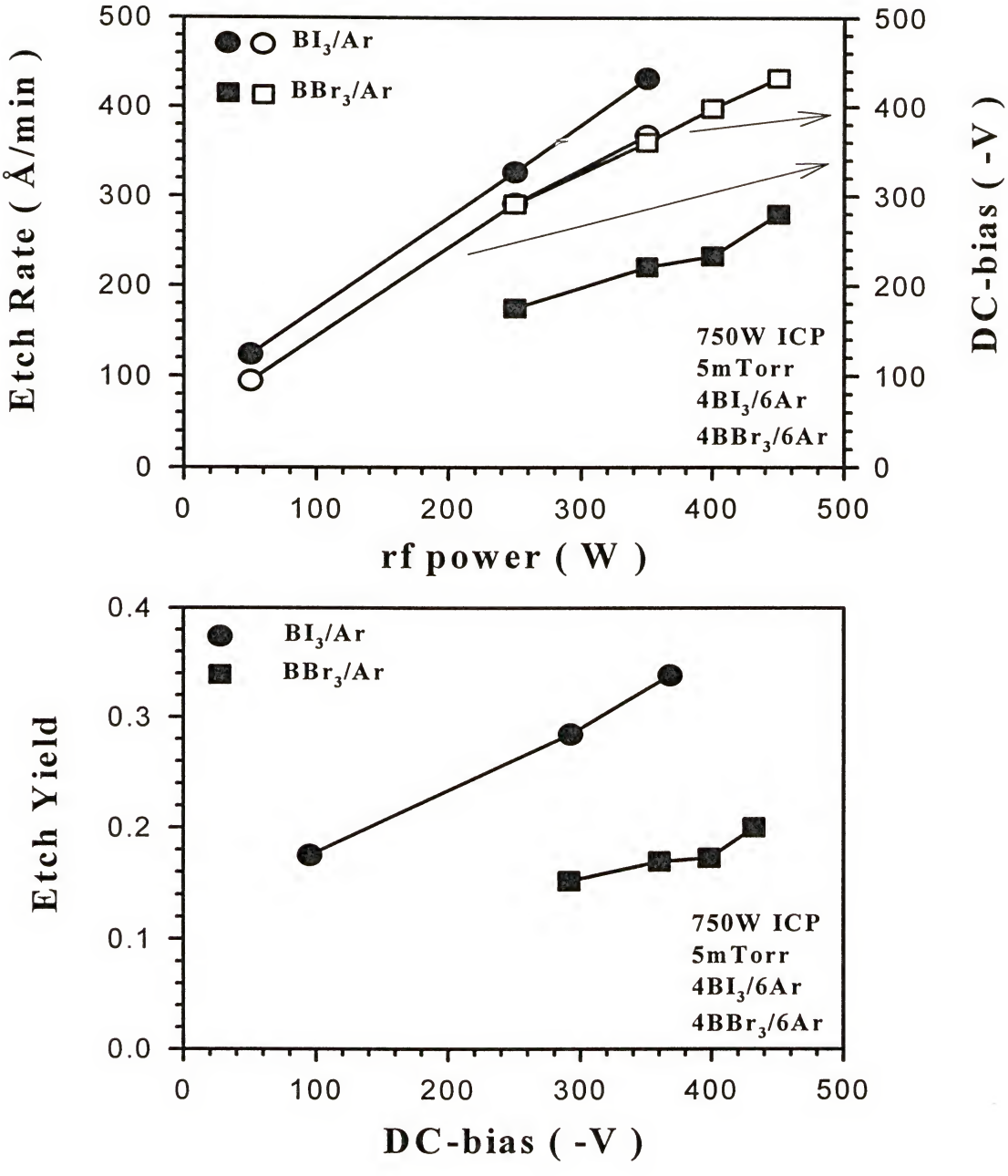

Figure 3-10 Etch rate (top) and etch yield (bottom) for $LaCaMnO_3$ in 750W ICP source power discharges of either $4BI_3/6Ar$ or $4BBr_3/6Ar$, as a function of rf chuck power (and hence dc bias).

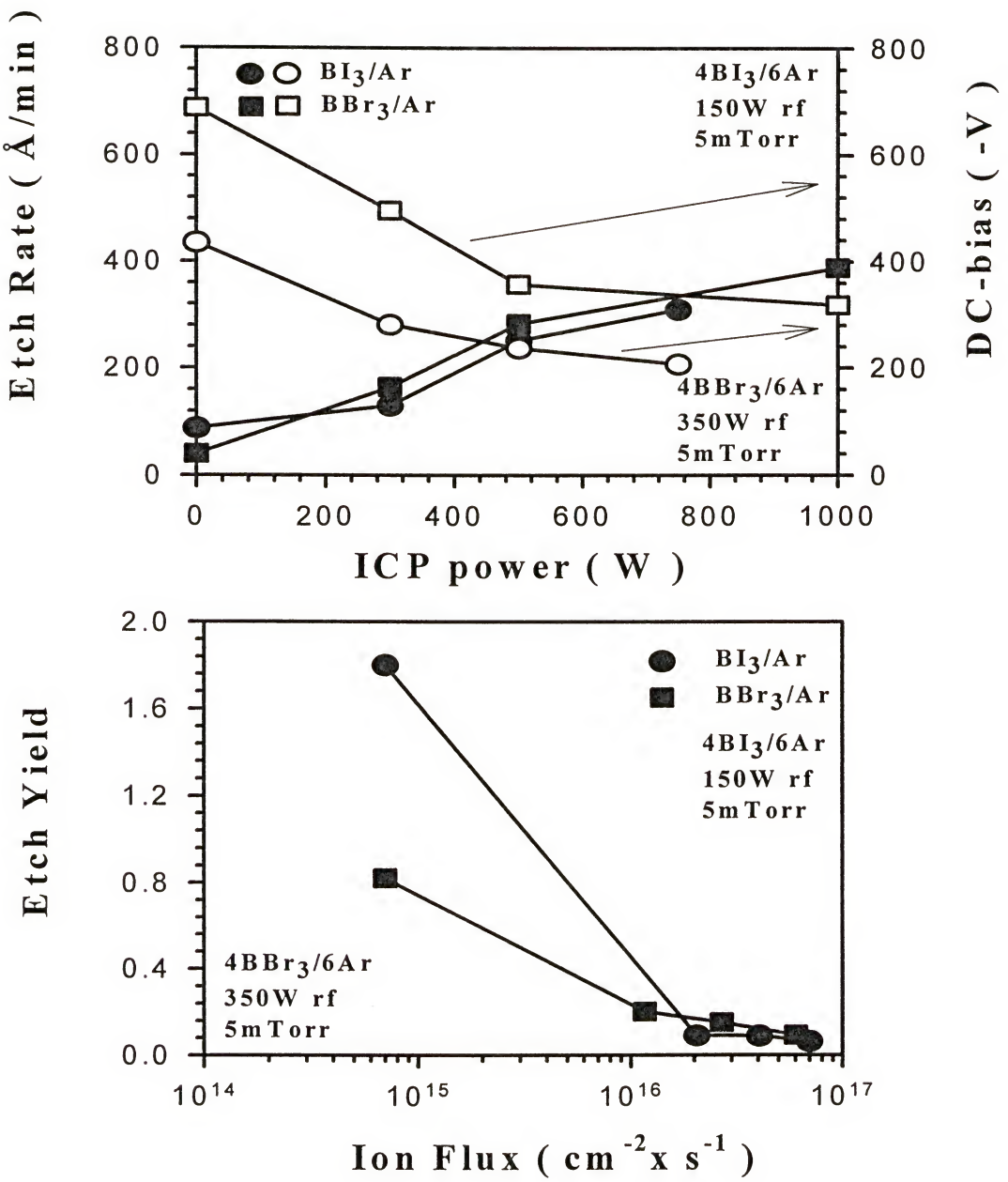

Figure 3-11 Etch rate (top) and etch yield (bottom) for $LaCaMnO_3$ in $4BI_3/6Ar$ or $4BBr_3/6Ar$ discharges as a function of ICP source power (and hence ion flux). The rf chuck power was 150W for the BI_3/Ar and 350W for the BBr_3/Ar.

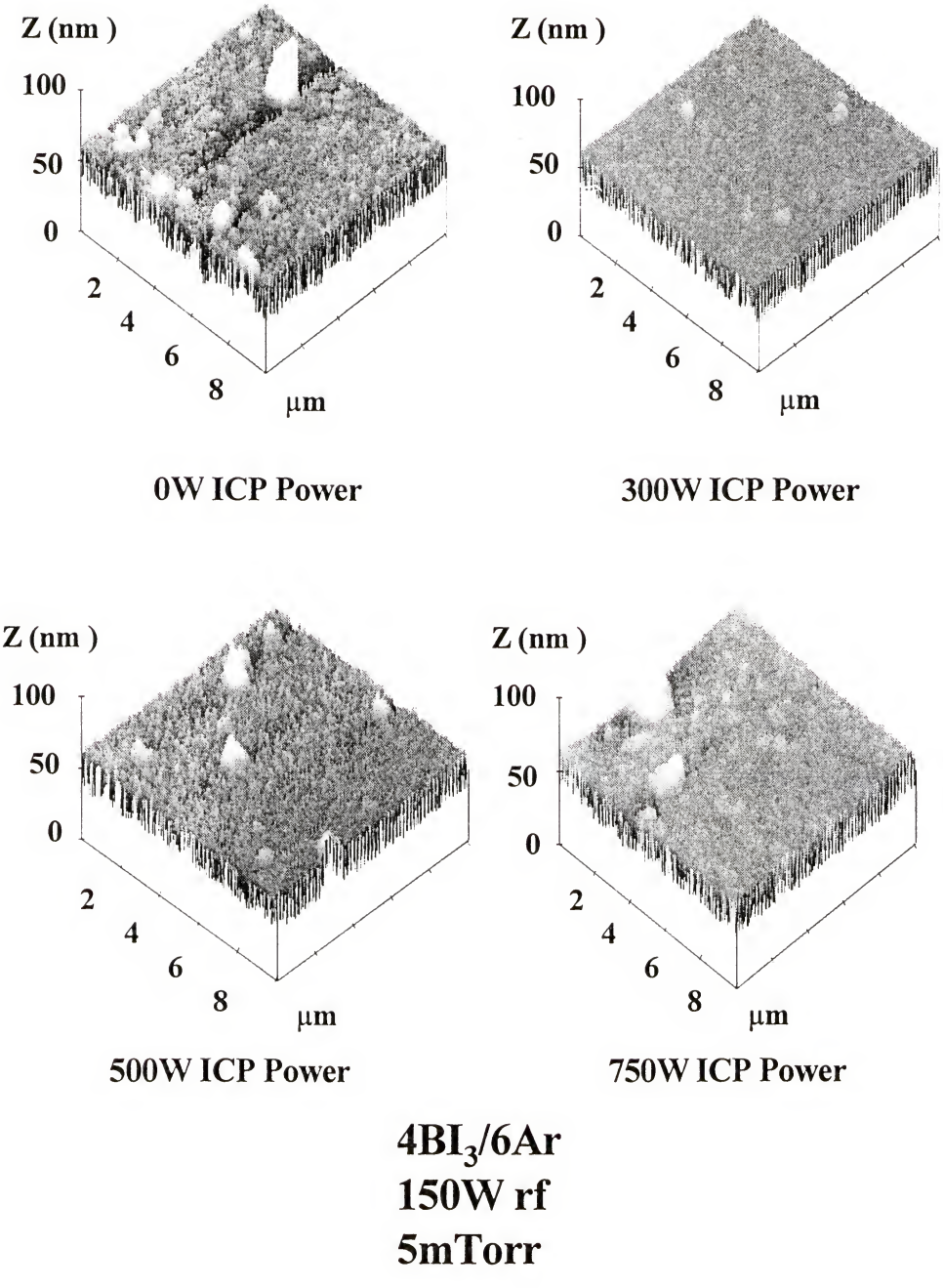

Figure 3-12 AFM scans of $LaCaMnO_3$ after etching in $4BI_3/6Ar$, 150W rf chuck power discharges, as a function of ICP source power.

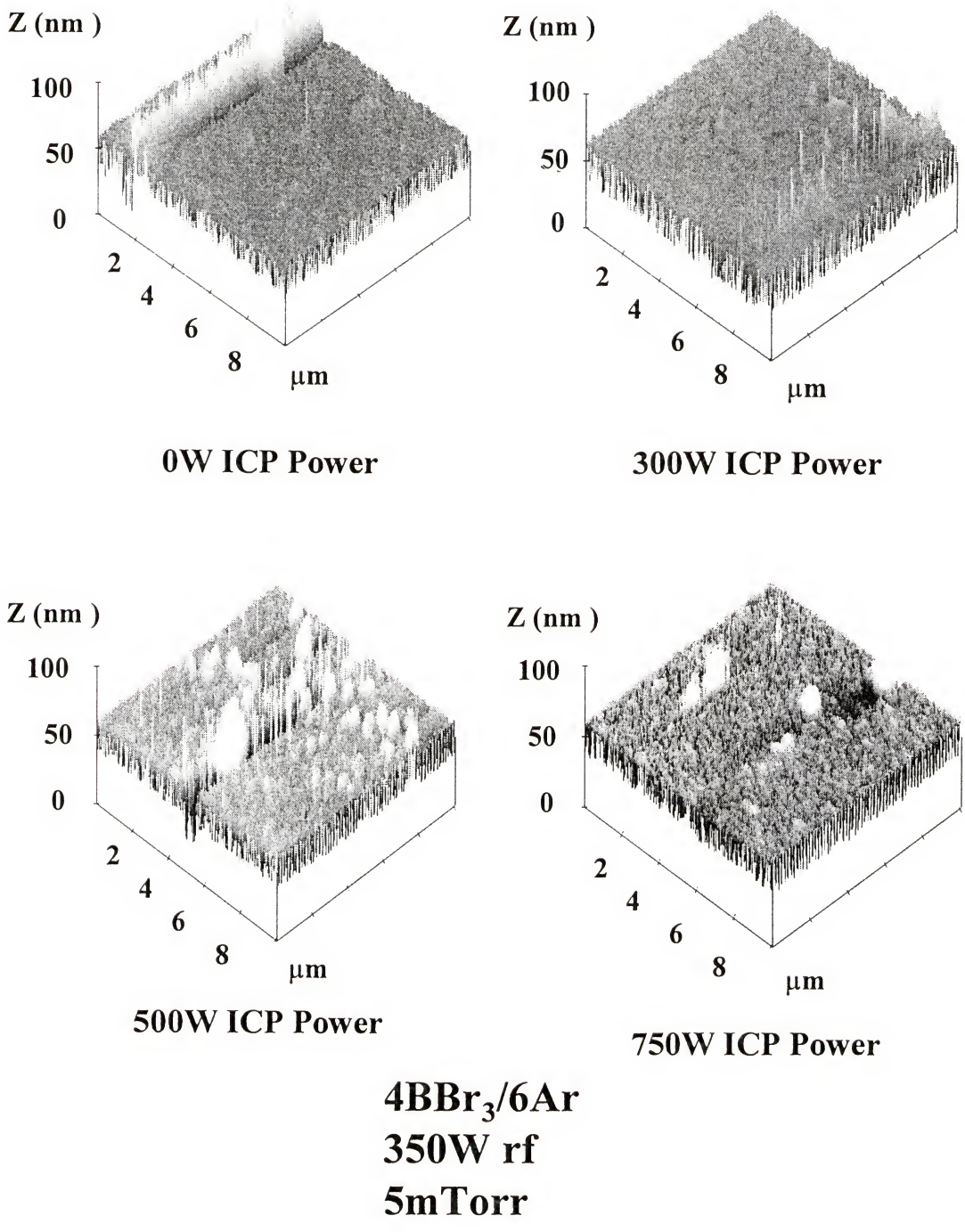

Figure 3-13 AFM scans of $LaCaMnO_3$ after etching in $4BBr_3/6Ar$, 350W rf chuck power discharges, as a function of ICP source power.

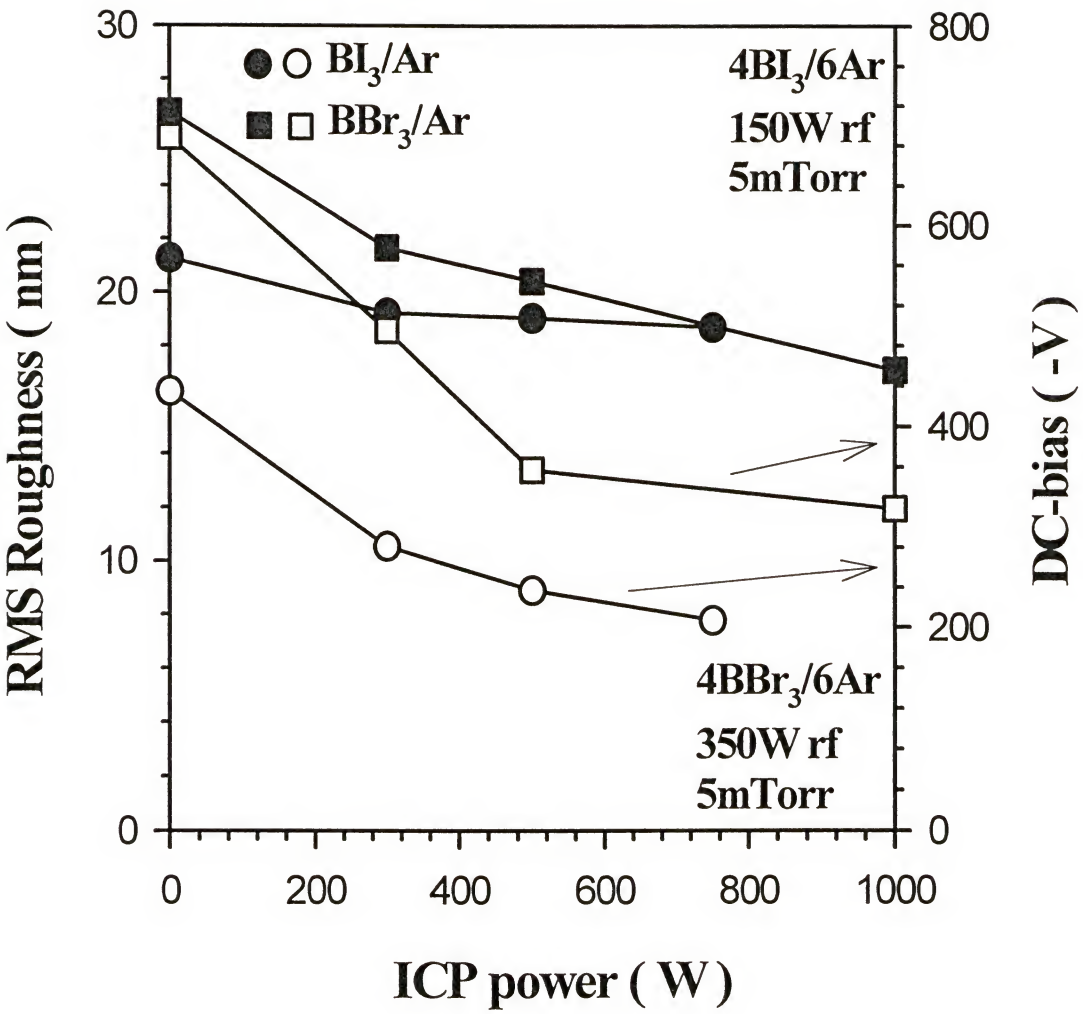

Figure 3-14 AFM RMS roughness for $LaCaMnO_3$ after etching in $4BI_3/6Ar$ or $4BBr_3/6Ar$ discharges as a function of ICP source power. The rf chuck power was 150W for the BI_3/Ar and 350W for the BBr_3/Ar.

Since the chemical component of the etching is relatively small, we would expect anisotropic pattern transfer. Figure 3-15 shows SEM micrographs of features etched into $LaCaMnO_3$ using either BI_3/Ar (top) or BBr_3/Ar (bottom) discharges and SiO_2 masks that were subsequently removed. The etched surface morphologies are again similar to those of the unetched regions, with slightly sloped sidewalls due to mask erosion. We have found that photoresist is typically not suitable as a mask material for high density plasma processes because the high ion currents lead to reticulation and loss of dimensional stability.[52] Figure 3-16 shows the BI_3/Ar and BBr_3/Ar etch selectivity for $LaCaMnO_3$ over both SiN_x and SiO_2 as a function of either source power (top) or rf chuck power (bottom). Note that the selectivities are generally less than one over a wide range of conditions, indicating that the etching is still dominated by the physical component.

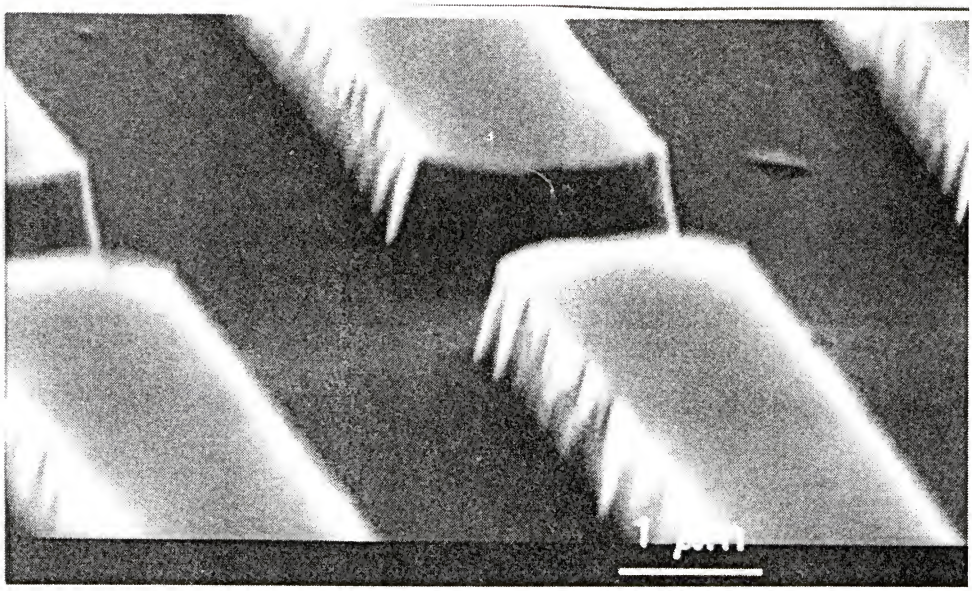

BI_3

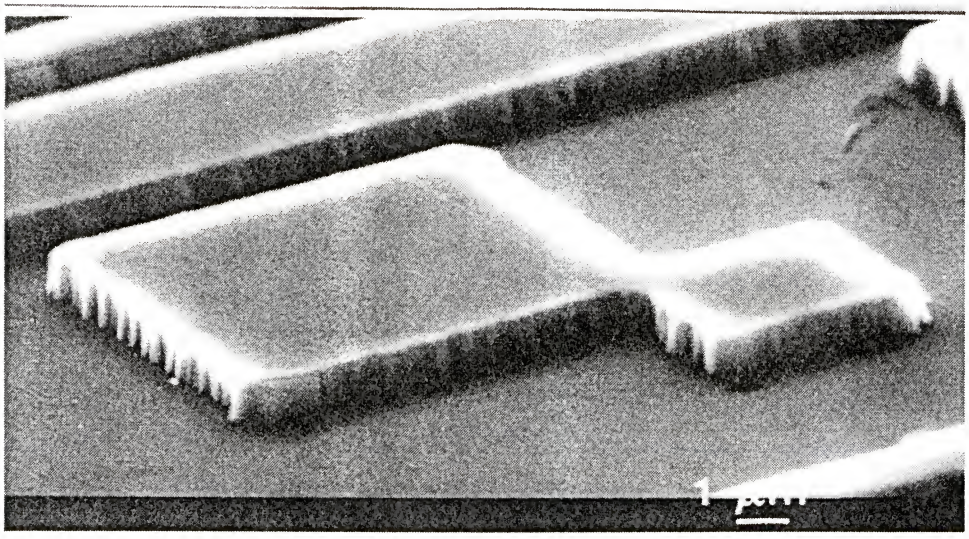

BBr_3

Figure 3-15 SEM micrographs of features etched into $LaCaMnO_3$ using either $4BI_3/6Ar$ (top) or $4BBr_3/6Ar$ (bottom) discharges with 750W of source power. The rf chuck power was 150W for the BI_3/Ar and 350W for the BBr_3/Ar. The SiO_2 masks have been removed from both samples.

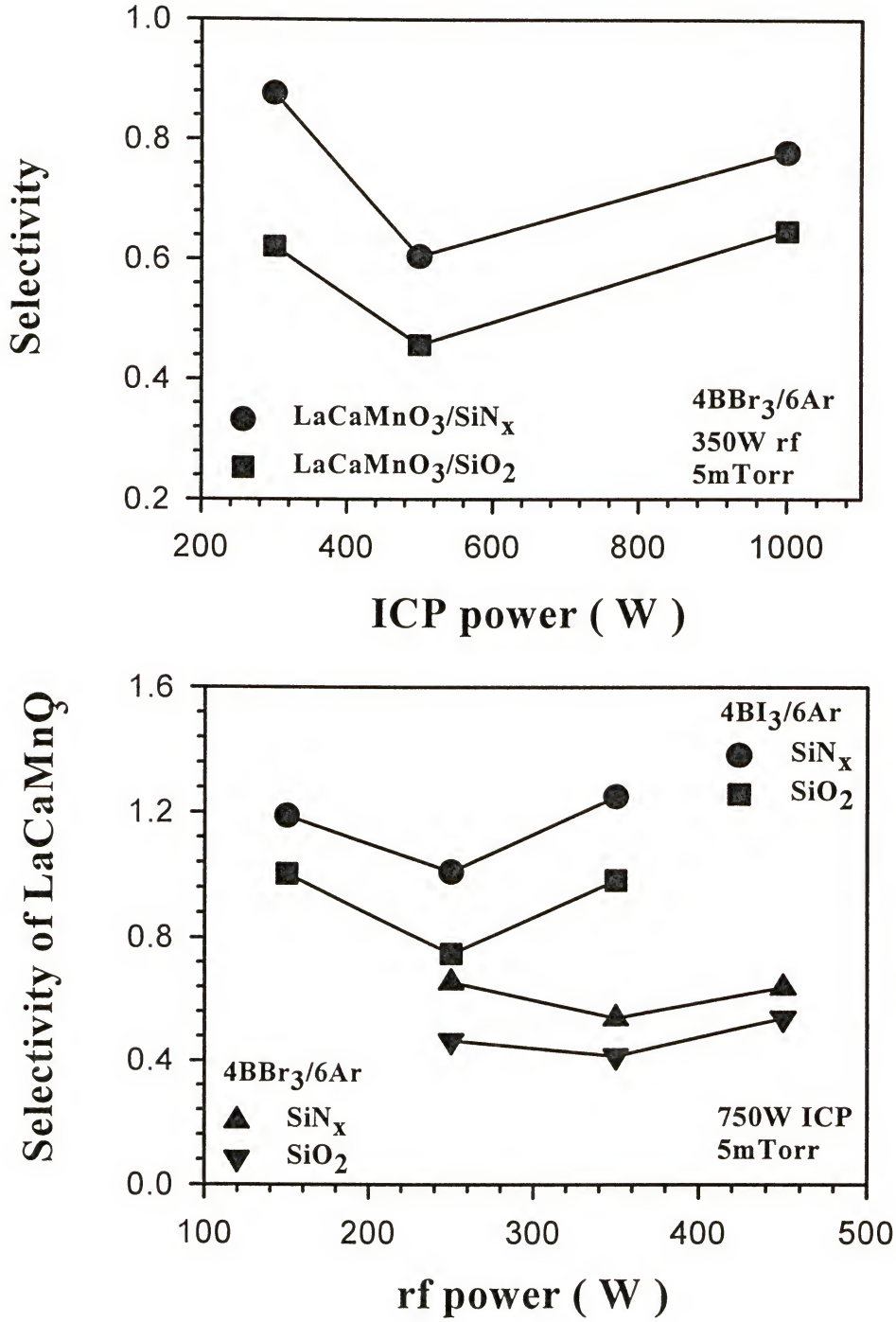

Figure 3-16 Etch selectivity for $LaCaMnO_3$ over SiO_2 and SiN_x as a function of either ICP source power (top) or rf chuck power (bottom).

CHAPTER 4
ETCHING SiC AND SiCN

4.1. Materials and Methods

The 6H-SiC substrates were 1 inch ϕ, doped with either Al ($p = 6\times10^{18}$ cm^{-3}) or N ($n \sim 5 \times10^{18}$ cm^{-3}), and both with Si face (0001) orientation, obtained from Cree Research. The X-ray diffraction full-width-at-half maximum is < 100 arc·sec. The $SiC_{0.5}N_{0.5}$ layers were grown on Si substrates using chemical vapor deposition with a tris-dimethylamino silane precursor, and were ~5,000 Å thick and nominally undoped. The X-ray diffraction full-width-at-maximum is typically > 400 arc·sec. Some of the samples were patterned with AZ5209E photoresist or ~3,000 Å thick indium tin oxide (ITO) masks. Flemish et_al.[53,54,55] have previously shown that ITO provides much better etch resistance during high density plasma processing of SiC with F_2-based mixtures than photoresist. All of the experiments were performed in a Plasma Therm 790 system. The samples are located on a He backside cooled chuck biased with 13.56MHz of power. The plasma is generated in a 2MHz, 1500W, 4-turn plasma coil geometry source and the pressure was held constant at 2mTorr. Electronic grade NF_3, O_2 and Ar gases were fed into the ICP source through mass flow controllers at total flow rates of 15 standard cubic centimeters per minute (sccm). Experimental process parameters were plasma composition, rf chuck power and ICP source power. Etch rates were obtained from stylus profilometry measurements of the samples after

mask removal. Scanning electron microscopy (SEM) was used to examine etch anisotropy and surface morphology, while tapping mode atomic force microscopy (AFM) was employed to quantify the surface roughness. Optical emission spectroscopy (OES) was used to monitor plasma species.

4.2. Results and Discussion

A common feature of fluorine-based plasmas under capacitively coupled conditions is that addition of O_2 at ratios by flow of 10-35% can increase the atomic fluorine neutral concentration.[56] We examined the optical emission spectra of both NF_3/O_2 and NF_3/Ar discharges, as shown in Figure 4-1. Surprisingly there was little significant difference in atomic fluorine concentration (confirmed by actinometric analysis using the 7451 nm Ar line), which suggests the ICP source is already very efficient in dissociating the NF_3. The spectra in Figure 4-1 also show little evidence of molecular continua, confirming the high dissociation efficiency.

These results are reflected in the etch rate data of Figure 4-2, which show SiC and SiCN removal rates as a function of NF_3 percentage in NF_3/O_2 and NF_3/Ar for fixed source power (750W), pressure and rf chuck power (250W). There are several interesting aspects of the data. First, the rates are slightly higher with NF_3/Ar, which suggests that ion bombardment plays a role in the etch mechanism. Since the etch products (SiF_x and CF_x, where $x \leq 4$) are quite volatile, it is likely that more efficient bond-breaking in the SiC rather than ion-enhanced desorption of these products, is the reason for this trend. Second, there is no measurable difference in etch rates between n^+ and p^+ SiC, indicating that Fermi level effects play no role in the etch mechanism. Third, the etch rates increase montonically with

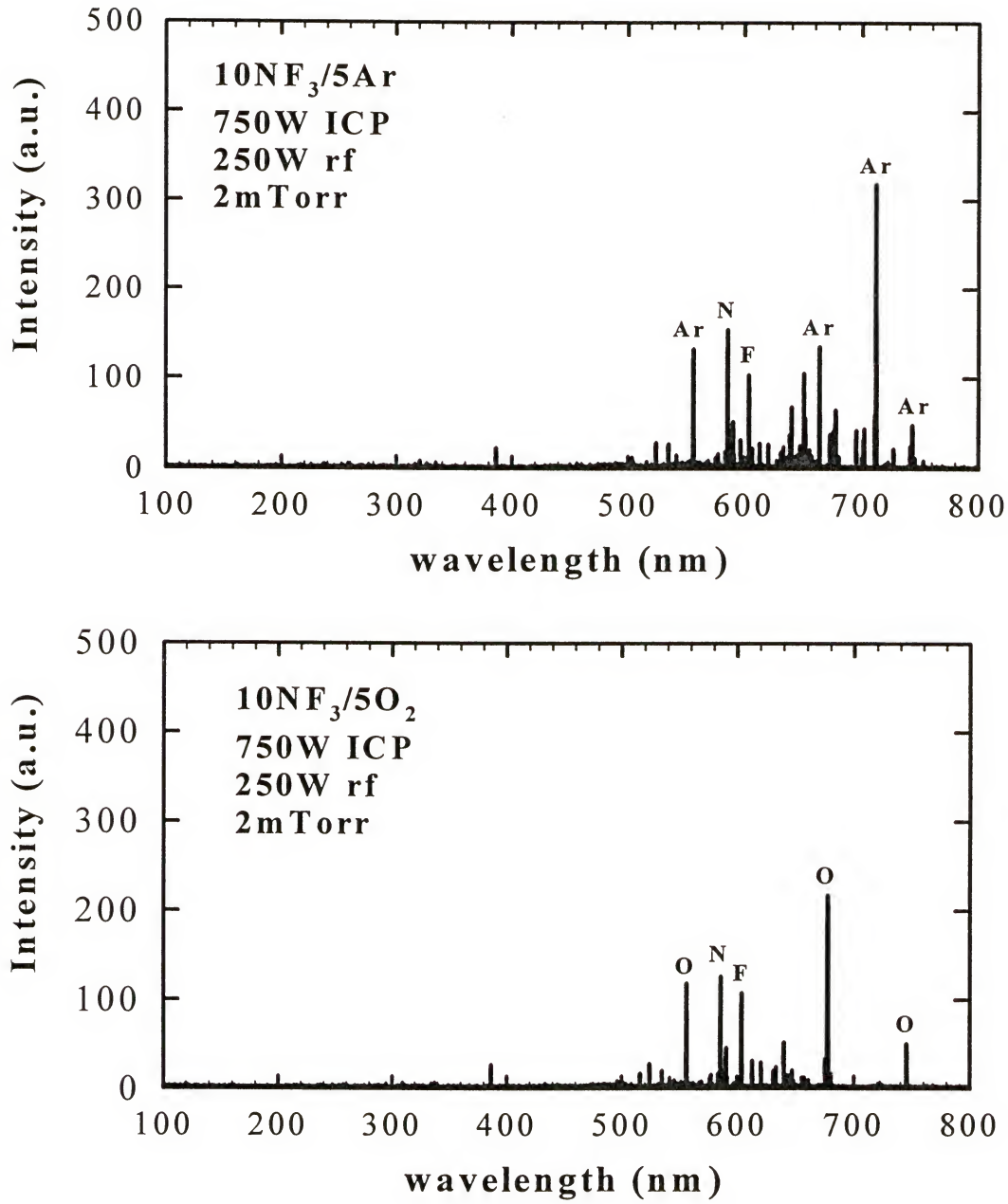

Figure 4-1 Optical emission spectra of ICP discharges (750W source power, 2mTorr, 250W rf power) of either $10NF_3/5Ar$ (top) or $10NF_3/5O_2$ (bottom).

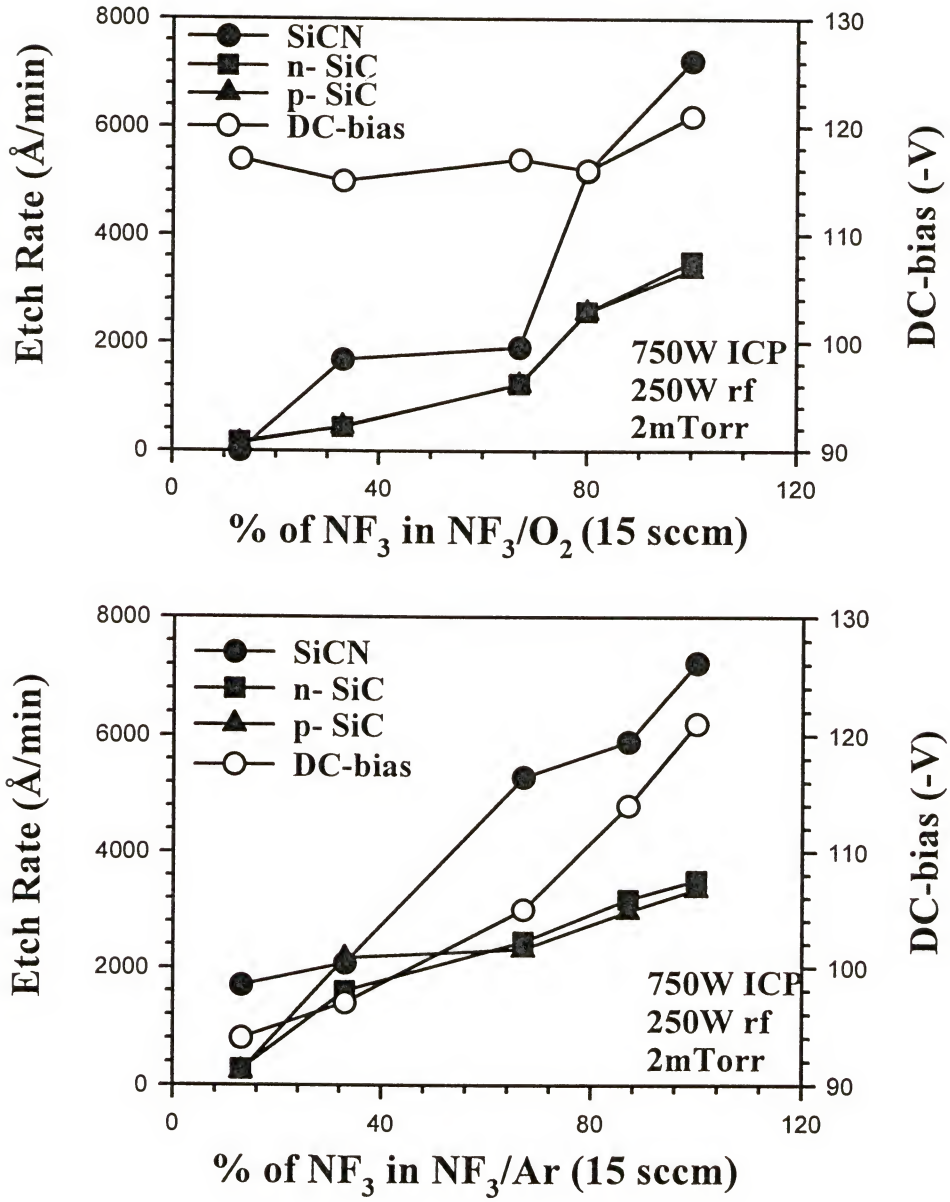

Figure 4-2 Etch rates of p^+ SiC, n^+ SiC and SiCN in 750W source power, 2mTorr,250W rf chuck power discharges as a function of NF_3 percentage in either NF_3/O_2 (top) or NF_3/Ar (bottom).

NF_3 percentage in both chemistries, which indicates that the limiting step is supply of atomic fluorine to the surface under these conditions. Fourth, the rates for SiCN are significantly higher than for SiC in both plasma chemistries, probably due to the high vapor pressure of the NF_x etch products and to the probable lower crystalline quality of the thin film SiCN relative to the bulk SiC, which is grown at much higher temperatures. Fifth, there is a finite etch rate for both materials in NF_3/Ar even at the lowest NF_3 percentage, whereas there is a threshold concentration for the commencement of etching in NF_3/O_2 discharges. Sixth, the behavior of dc self-bias with plasma composition is quite different in the two plasma chemistries. While it stays relatively constant in NF_3/O_2 suggesting that ion density also remains approximately constant, there is a monotonic increase with NF_3 percentage in NF_3/Ar. In the latter case this indicates that the conductivity of the plasma is decreasing as NF_3 increases, leading to a higher self-bias. The associated higher ion energy is also a contributing factor to the higher etch rates with NF_3/Ar relative to NF_3/O_2.

Figure 4-3 shows etch rates as a function of rf chuck power (top) and etch yield as a function of dc self-bias (bottom). The etch yield is the number of molecules of the substrate removed per incident ion. For SiC there is a monotonic increase in etch rate with bias, which again emphasizes the strong role of ion energy in the etch mechanism. The average ion energy is the sum of the dc self-bias voltage and plasma potential (roughly ~ 20V in this tool). For SiCN the etch rate saturates as this bias is increased and this may be related to sputter-induced removal of the atomic fluorine before it can react with the surface. Note that the etch yields are relatively low, but the resulting etch rate is high because of the high ion flux.[57]

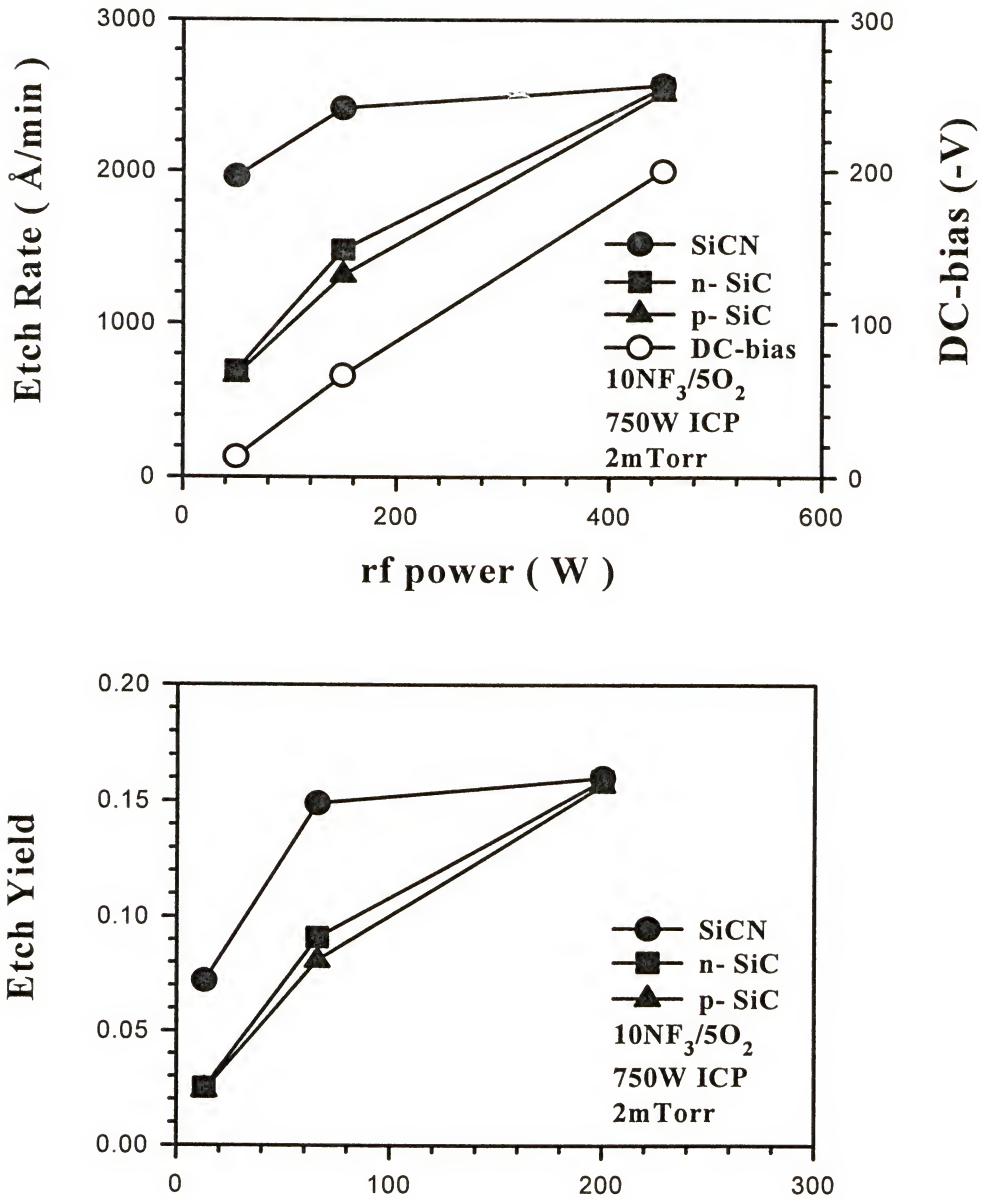

Figure 4-3 Etch rates of SiC and SiCN as a function of rf chuck power in $10NF_3/5O_2$, 2mTorr, 750W source power discharges (top) and etch yield of the same materials as a function of dc chuck self-bias (bottom).

Figure 4-4 shows the dependence of etch rates on ICP source power (top) and the etch yield versus ion flux (bottom). As the source power is increased at constant rf chuck power, the dc self-bias is strongly suppressed and the competing factors of increasing ion flux and decreasing ion energy produce the resulting maximum in etch rate at ~ 1000W source power. Note that the etch rate for SiC can still be above 1,000 Å/min even at very low bias values provided the ion flux is high.[57]

Some typical SEM micrographs of features etched into p^+ SiC under different conditions are shown in Figure 4-5. At top (left and right) are features from samples etched with $5NF_3/10Ar$, 2mTorr, 500W source power, 300W rf chuck power discharges, using an ITO mask which was subsequently removed. The features are quite anisotropic and the etched surface is smooth. There is some slight degree of trenching at the base of the sidewalls, which was also reported by Flemish et_al.[53,55,58] for ECR CF_4-based etching of SiC and is usually ascribed to glancing angle collisions of ions with the sidewall that produce enhanced etching at the foot of the sidewall. The two micrographs at bottom show problems that can arise if the plasma conditions are chosen to overly emphasize either the physical or chemical components of the etching. The feature at bottom left was formed by etching in a $15NF_3$, 2mTorr,750W ICP source power, 450W rf chuck power plasma. The combination of high ion flux and high ion energy produce substantial facetting of the ITO mask, which is still in place. This leads to sloped sidewalls and trenching at the foot of the picture. By contrast, if ion energy is reduced under these conditions by lowering of chuck power to 250W, the chemical component of the etching is enhanced and leads to significant sidewall undercut (Figure 4-5, bottom right) It is clearly necessary to balance the physical and chemical contributions in order to optimize the anisotropy of the etched features.

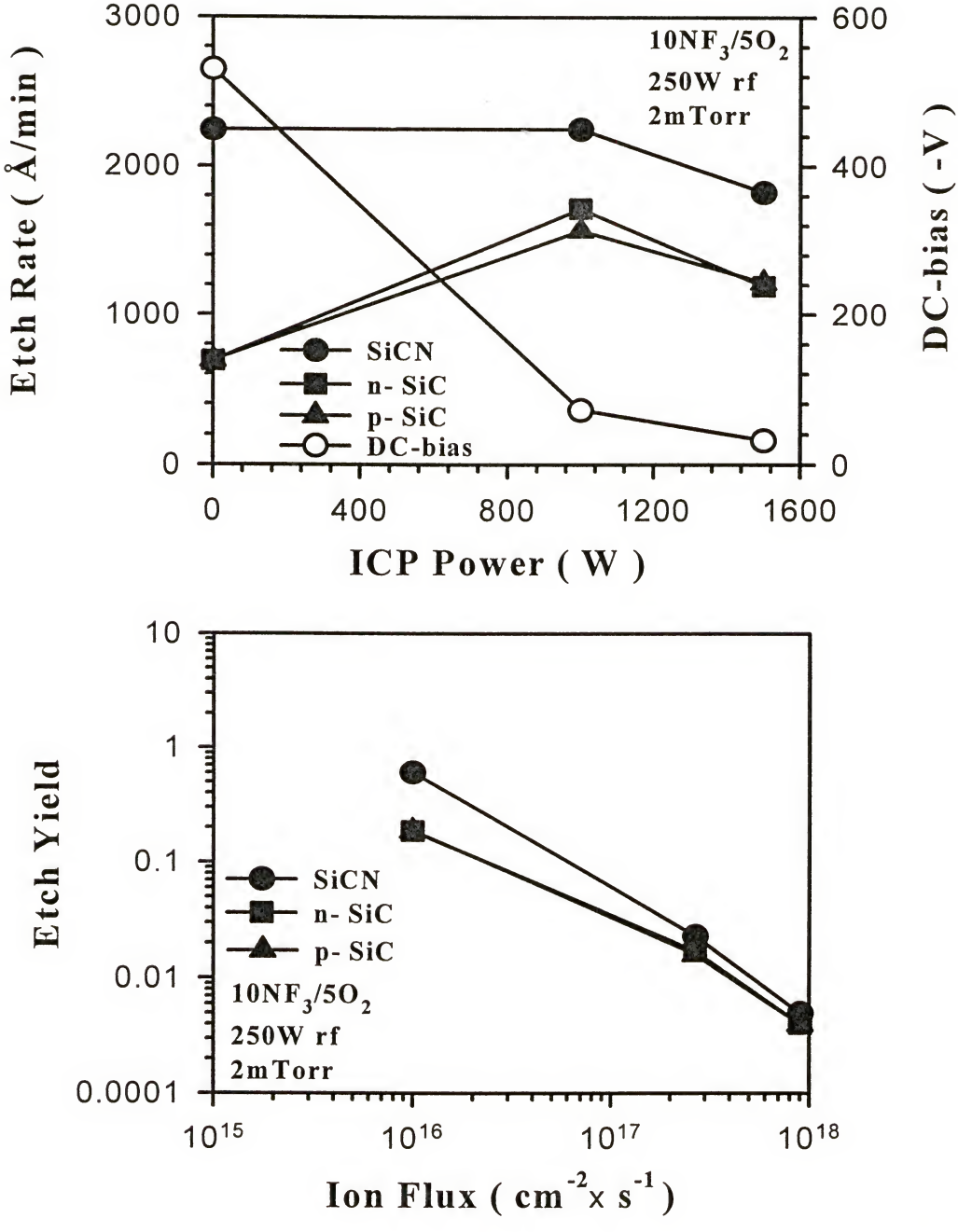

Figure 4-4 Etch rates of SiC and SiCN as a function of source power in $10NF_3/5O_2$, 2mTorr, 250W chuck power discharges (top) and etch yield of the same materials as a function of ion flux (bottom).

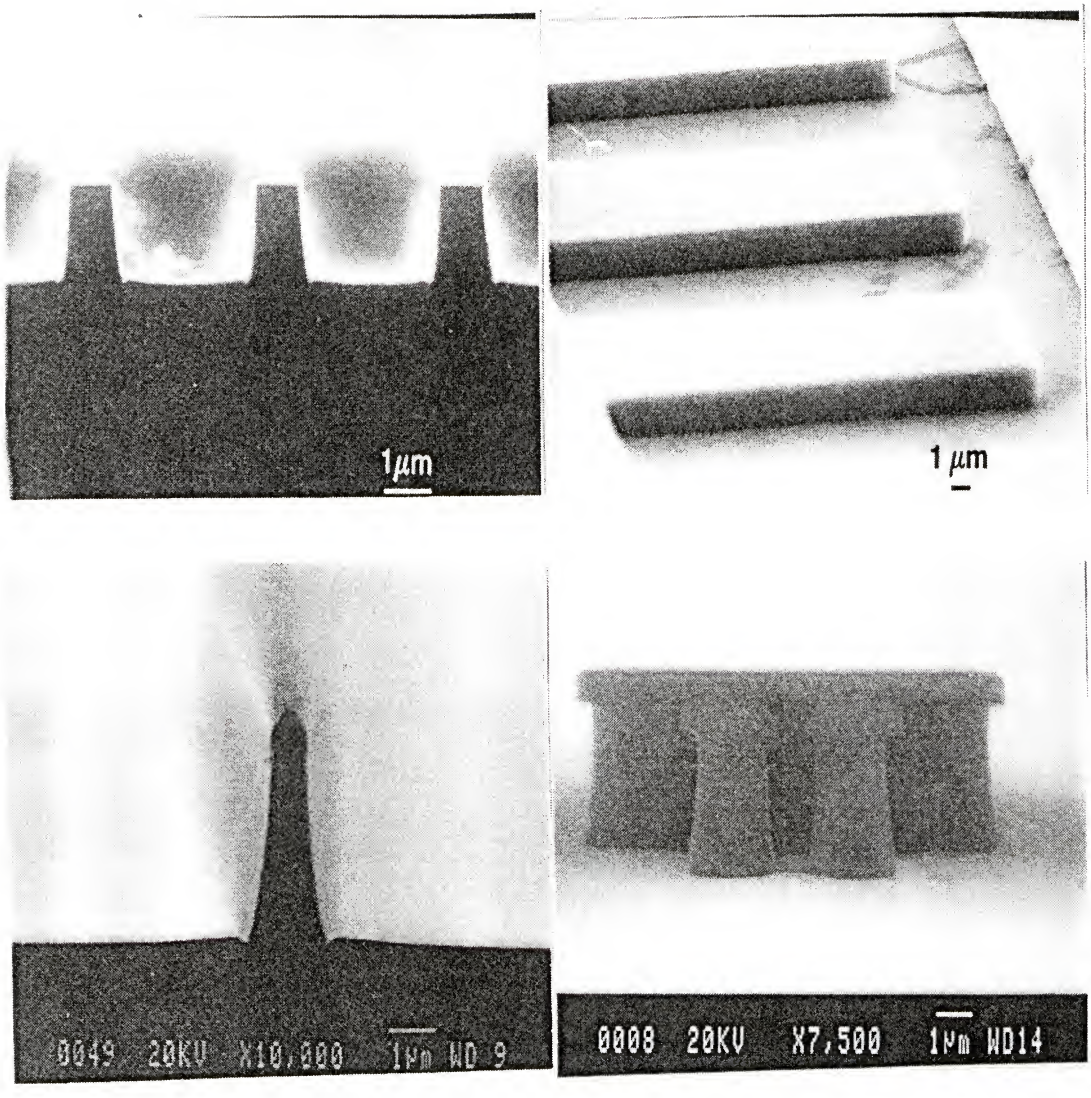

Figure 4-5 SEM micrographs of features etched into p^+ SiC using $5NF_3/10Ar$, 2mTorr, 500W source power, 300W rf chuck power discharges (top left and right) or$15NF_3$, 2mTorr, 750W source power discharges with either 450W chuck power (bottom left) or 250W chuck power (bottom right).

The surface roughness of both SiCN and SiC was examined after etching by AFM. Figure 4-6 shows some representative scans for SiCN films etched in NF_3/O_2 discharges, as a function of gas composition for fixed source power, pressure and chuck power. The morphologies are clearly worse at higher NF_3 percentages. By sharp contrast, the surfaces of both n^+ and p^+ SiC were relatively unaffected by discharge composition, as shown for both materials in Figures 4-7 and 4-8 respectively. There is clearly some structure to the surfaces, but at all conditions they are still relatively smooth. The plasma composition dependence of root–mean–square (RMS) roughness is plotted in Figure 4-9 for SiCN, n^+ SiC and p^+ SiC. The values for SiCN go through a minimum at ~33% NF_3 by flow in NF_3/O_2, and become very high as the NF_3 percentage is increased.

The surfaces of the etched SiC were chemically clean over a very broad range of conditions, as shown in the AES surface scans of Figure 4-10. In all cases the SiC samples showed stoichiometric surfaces over the whole range of plasma compositions, with very small quantities ($\leq$0.2 at%) of N- or F- containing residues in some cases. This indicates that Si and C are being removed at equal rates under a wide range of conditions and that the etch products, once formed, are readily leaving the surface. The oxygen signals originates from the presence of a native oxide due to atmospheric exposure during transfer of the samples from the etch reactor to the AES analysis system. We did not perform Auger Electron Spectroscopy (AES) in SiCN samples, but we suspect that the surface becomes non-stoichiometric through preferential loss of one of the lattice constituents (probably N because NF_3 is the most volatile of the prospective etch products).

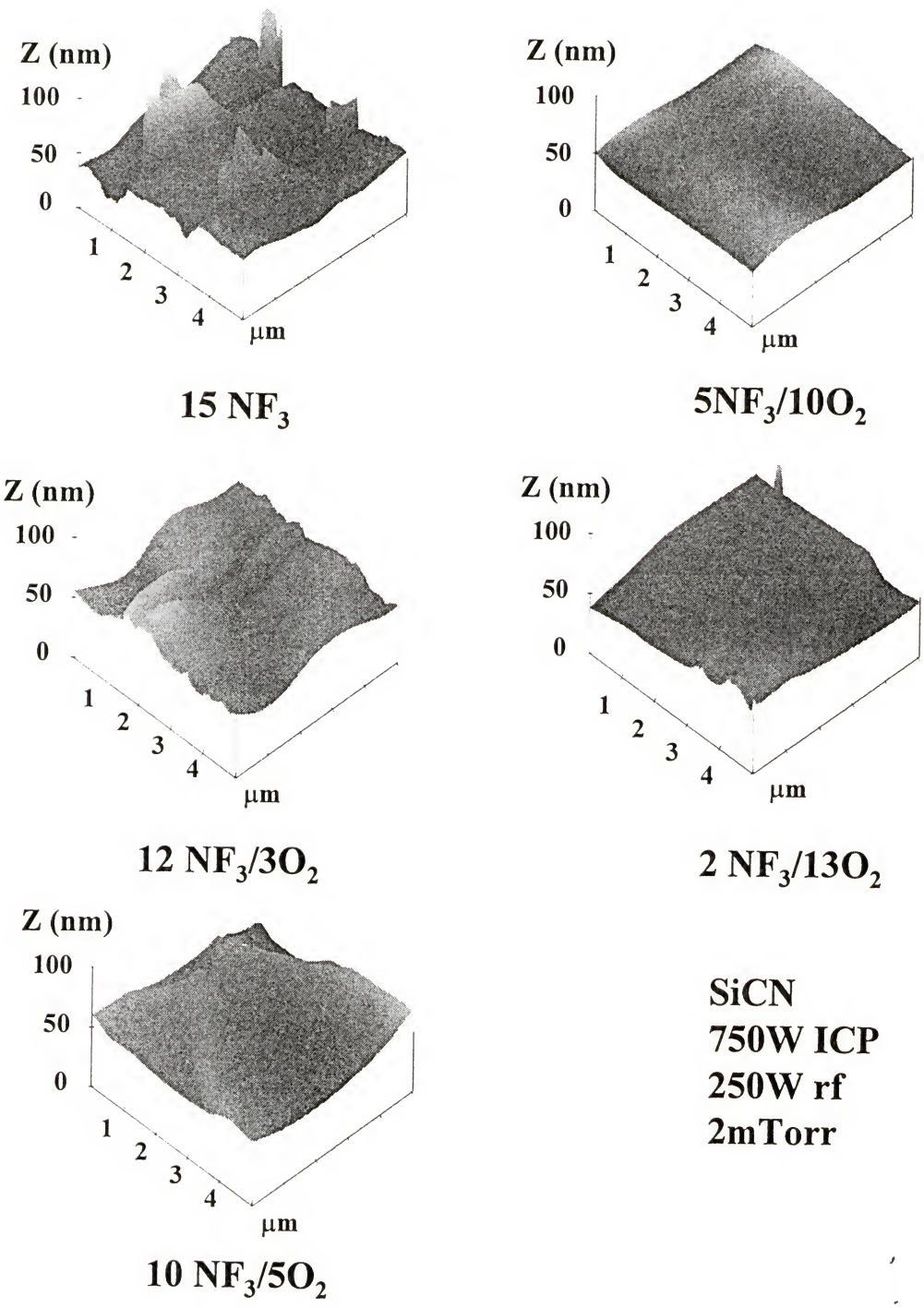

Figure 4-6 AFM surface scans of SiCN films etched in NF_3/O_2 discharges (750W source power, 250W rf chuck power, 2mTorr) as a function of plasma composition.

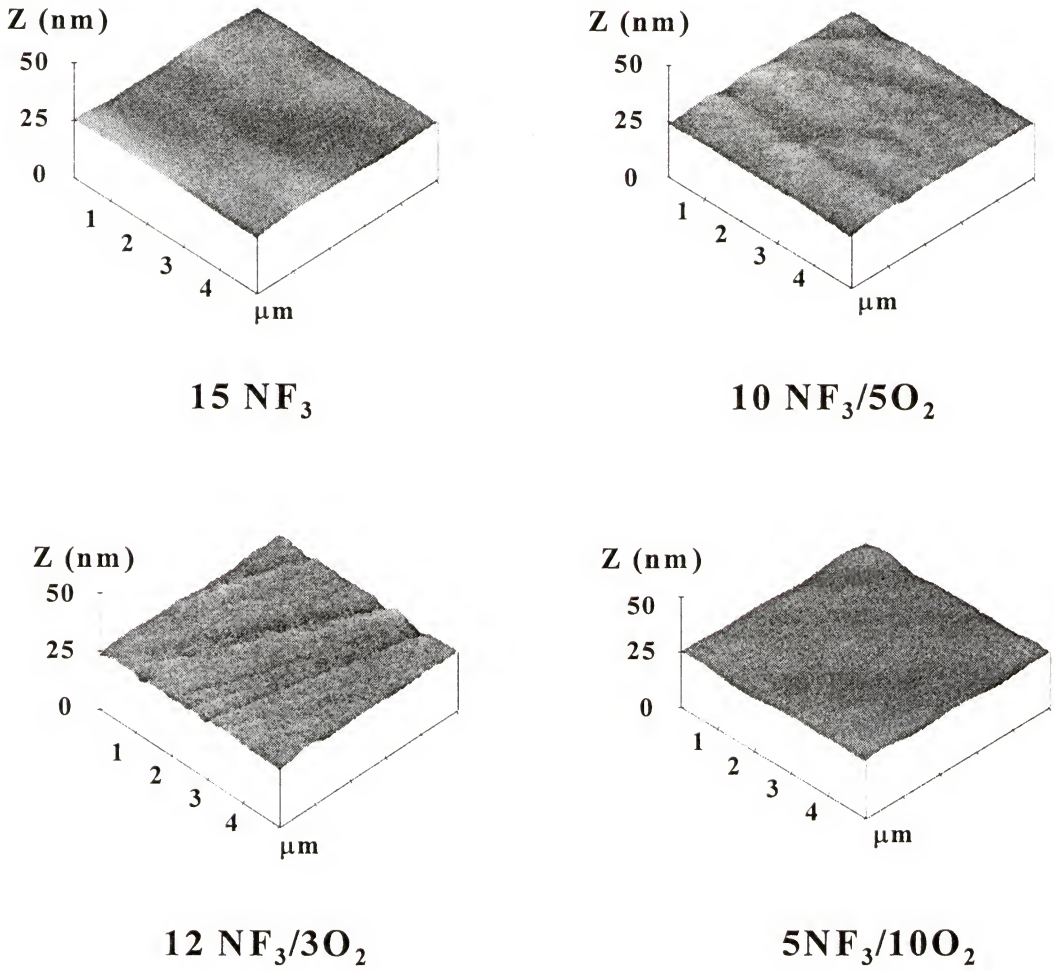

Figure 4-7 AFM surface scans of n^+ SiC etched in NF_3/O_2 discharges (750W source power, 250W rf chuck power, 2mTorr) as a function of plasma composition.

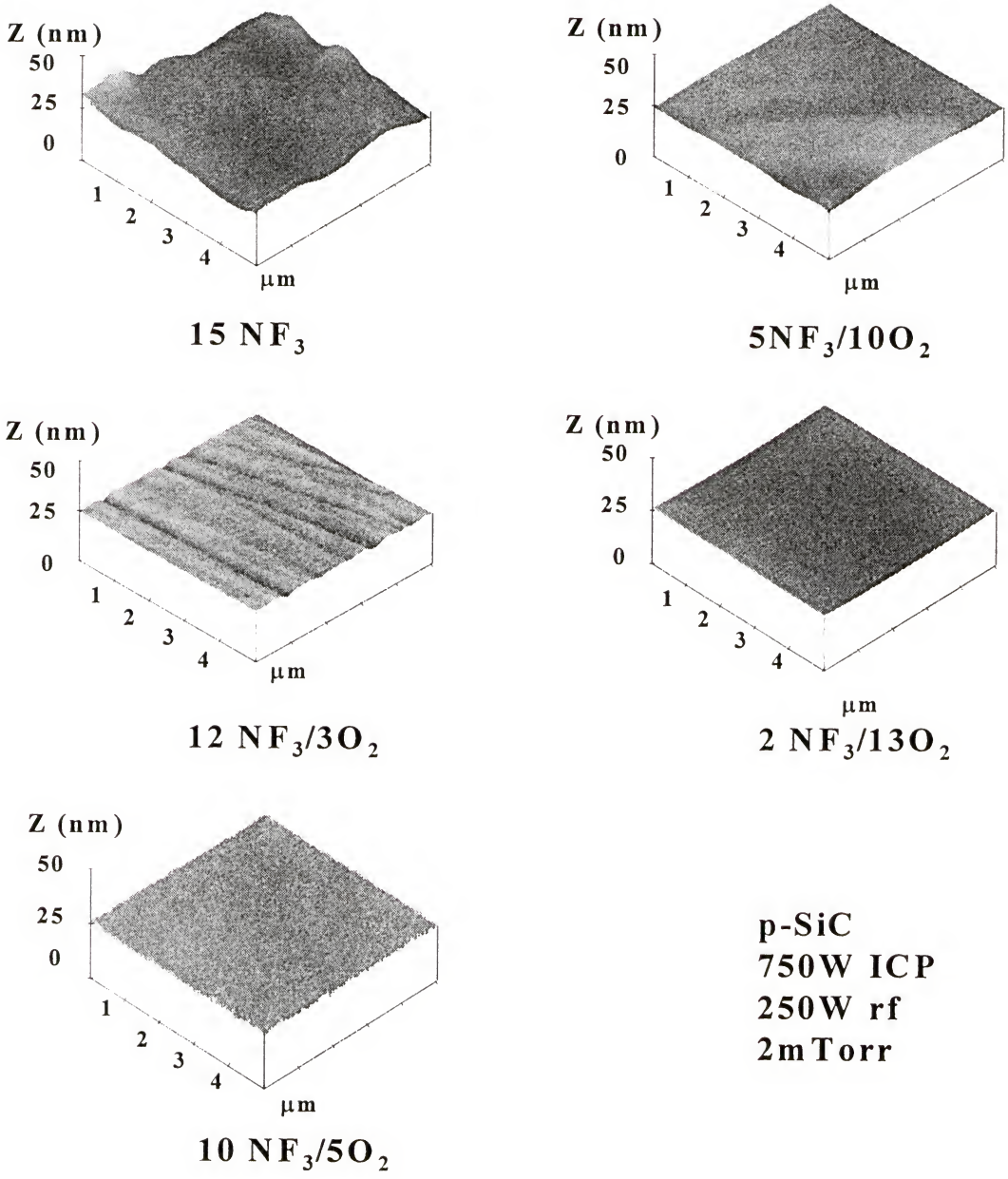

Figure 4-8 AFM surface scans of p^+ SiC etched in NF_3/O_2 discharges (750W source power, 250W rf chuck power, 2mTorr) as a function of plasma composition.

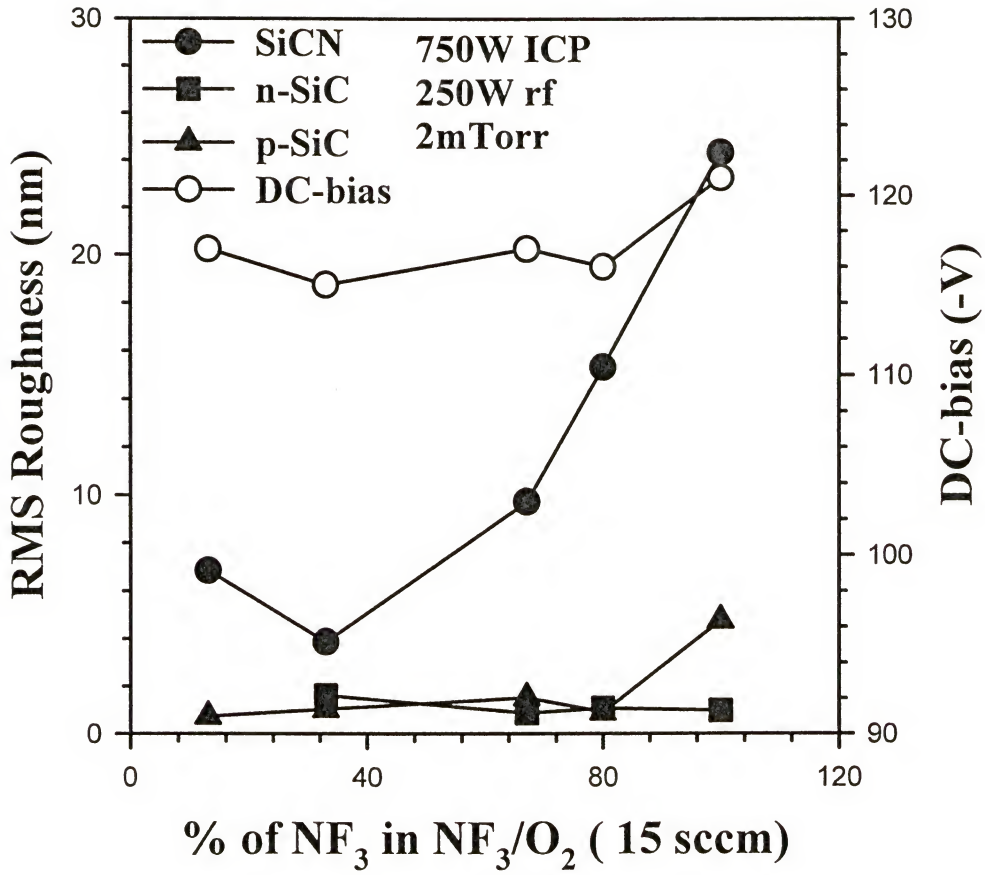

Figure 4-9 RMS roughness of SiC, n^+ and p^+ SiC measured by AFM after etching in NF_3/O_2 discharges (750W source power, 250W rf chuck power, 2mTorr) as a function of plasma composition.

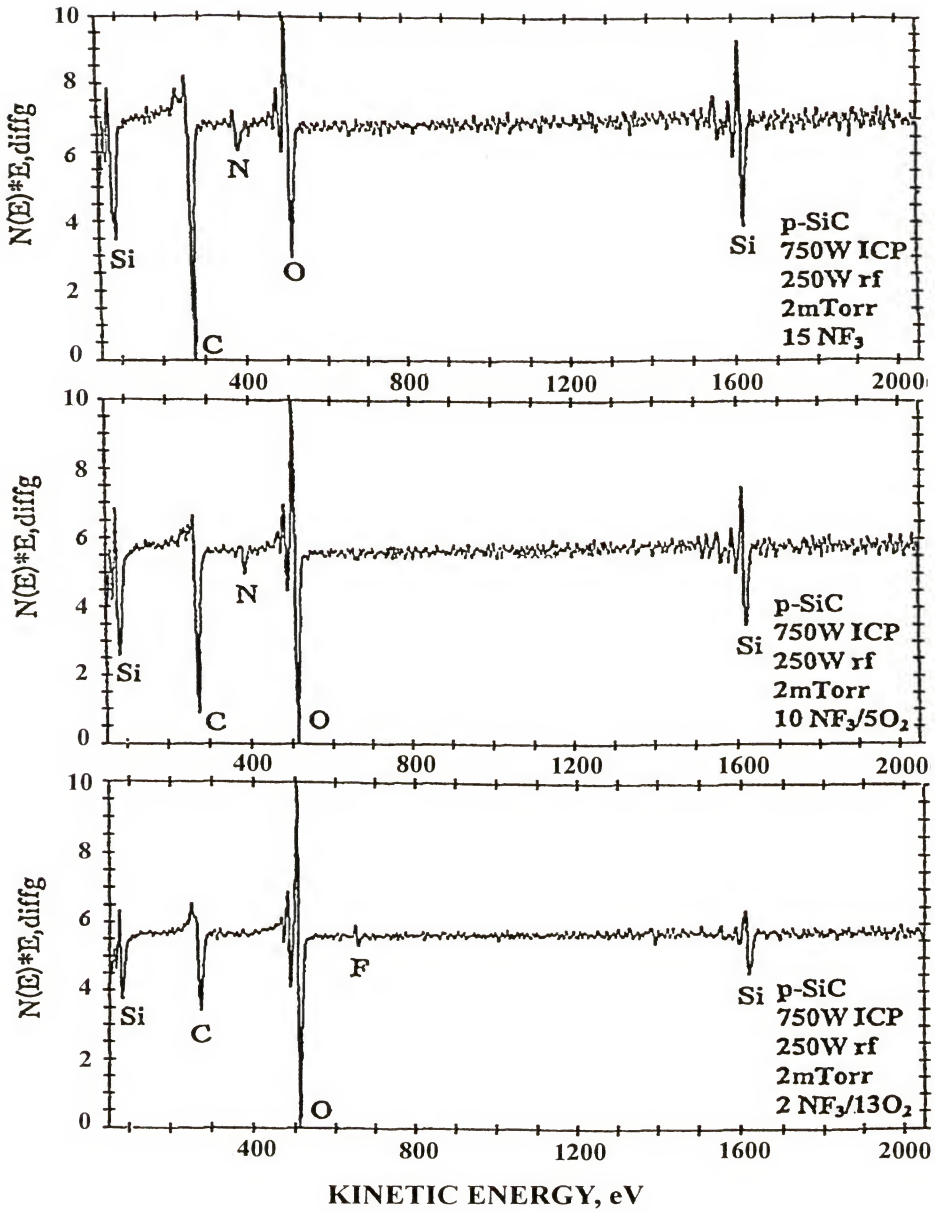

Figure 4-10 AES surface scans from n^+ SiC after etching in 2mTorr, 750W source power,250W rf chuck power discharges of $15NF_3$ (top), $10NF_3/5O_2$ (center) or $2NF_3/13O_2$ (bottom).

A final issue of practical interest is the etch selectivity of the SiC with respect to the two mask materials, photoresist and ITO. Figure 4-11 shows this data as a function of source power in $10NF_3/5O_2$, 2mTorr, 250W rf chuck power discharges. As expected there is no selectivity with respect to photoresist, but the ITO has excellent etch resistance,[55] which increases as source power is increased due to the associated reduction in ion energy. A basic problem with dry etching of SiC is that the F-based chemistries which are most effective have poor selectivity for SiO_2, SiN_x and resist, requiring the use of non-standard mask materials.

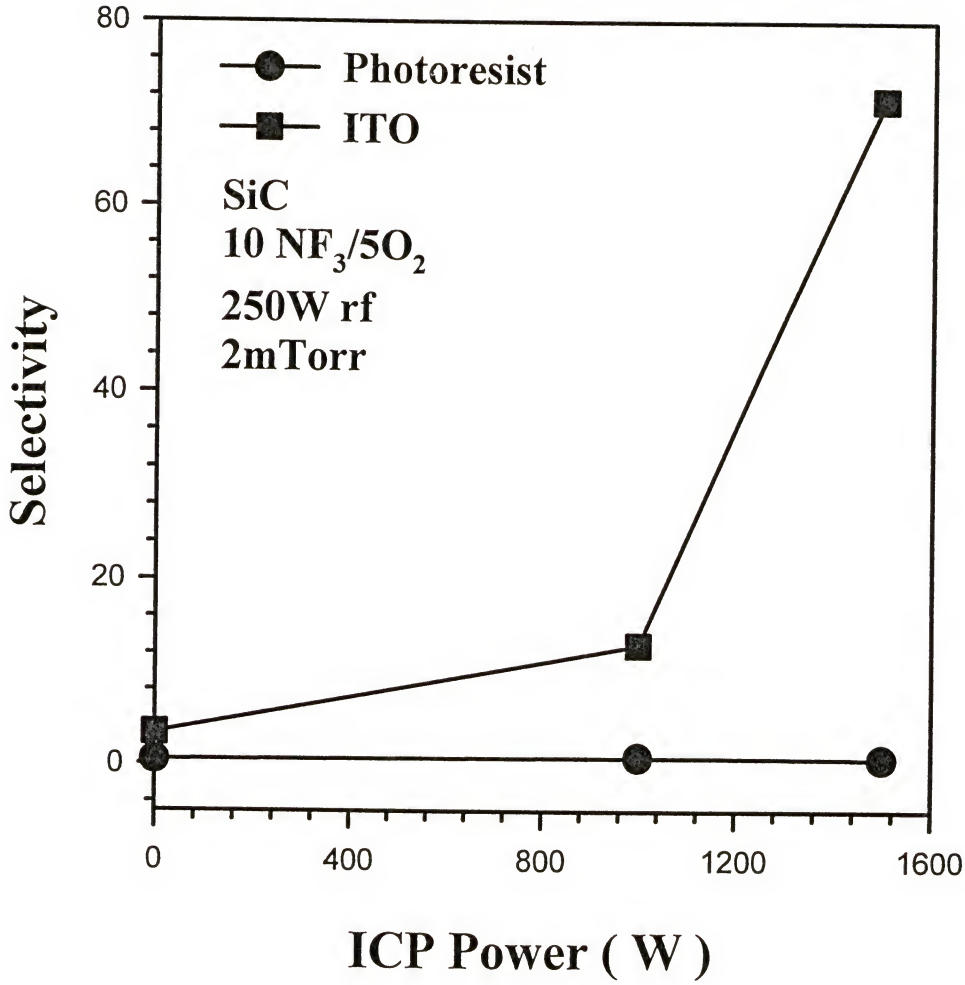

Figure 4-11 Etch selectivity for SiC relative to ITO and photoresist as a function of ICP source power in $10NF_3/5O_2$, 250W chuck power, 2mTorr discharges.

CHAPTER 5
SUMMARY

As predicted by the volatilities of the potential etch products, plasma chemistries based on Cl_2, F_2 or CH_4/H_2 did not show any degree of chemical enhancement for etching of $LaCaMnO_3$. Use of I_2- or Br_2-based mixtures provides a small degree of chemical enhancement relative to pure Ar sputtering. For this material, it is a disadvantage to use simple Ar ion milling for pattern transfer processes at modest acceleration voltages in order to avoid preferential sputtering effects if deep features are required, because the associated mask thickness would need to be similar to the etch depth in the $LaCaMnO_3$. Smooth, anisotropic pattern transfer is achieved under ECR and ICP plasma conditions. The etch rates are a strong function of plasma composition, ion flux and ion energy. Ion-to-neutral ratios on order 0.02 are available under ICP conditions based on I_2 or Br_2 plasma chemistries (much higher than in conventional RIE tools, $\sim 10^{-6}$), and provide the ability to enhance the desorption of otherwise involatile etch products. However it is still problematic as to whether there is sufficient advantage gained by using BI_3 and BBr_3 relative to pure Ar sputtering to justify the extra precautions needed in handling these corrosive materials. By contrast, chemical etch enhancements relative to pure Ar sputtering were obtained for SmCo with Cl_2/Ar over the whole range of dc self-biases examined and with SF_6/Ar at low biases (up to approximately -200V). The sidewalls on

etched features were again vertical, and the etched field quite smooth. Selectivities as high as ~ 12 were obtained for SmCo with respect to SiO_2 and SiN_x in Cl_2/Ar discharges.

ICP NF_3-based discharges produce smooth pattern transfer in SiC and SiCN at high rates (~3,500 Å/min in both n^+ and p^+ SiC, and ~7,500 Å/min in SiCN thin films.) The surface morphology of SiC was essentially independent of plasma composition in NF_3/O_2 discharges, but SiCN was much more sensitive to the atomic fluorine concentration. The etch rates of both SiC and SiCN were strong functions of ion flux, ion energy and fluorine concentration. This is consistent with the idea that the initial bond-breaking in the materials is an important step in the etch mechanism and this is enhanced at high ion fluxes and ion energies . Provided that there are sufficient weakened or broken bonds available for atomic fluorine to bond to , then the concentration of this reactant becomes the limiting step. The advantage of using NF_3 is that it is more readily dissociated than CF_4 or SF_6 and the combination with an ICP source means that ion energy, ion flux and atomic neutral density can be readily adjusted to produce high fidelity pattern transfer. ITO is an excellent mask material when etching deep (>2 μm) features, since selectivities of SiC to photoresist are only ~2:1.

LIST OF REFERENCES

1. M.N. Baibich, J.M. Broto, A. Fert, F. Nguyen Van Dau, F. Petroff, P. Etienne, G. Creuzet, A. Friederich and J. Chazelas, Phys. Rev. Lett. 66, 2472 (1988).

2. R. von Helmolt, J. Wecker, B. Holzapfel, L. Schultz and K. Samwer, Phys. Rev. Lett. 71, 2331 (1993).

3. C.E. Weitzel, J.W. Palmour, C.H. Carter, Jr. K. Moore, K.J. Nordquist, S. Allen, C. Thero and M. Bhatanagar, IEEE Trans. Electron. Dev. 43 1732 (1996).

4. K.Z. Xie, J.H. Zhao, J.R. Flemish, T. Burke, W.R. Buchwald, G. Lorenzo and H. Singh, IEEE Electron. Dev. Lett. 17 142 (1996).

5. B.J. Baliga, IEEE Trans. Electron. Dev. 43 1717 (1996).

6. A.K. Agarwal, G. Augustine, V. Balakrishna, C.D. Brandt, A.A. Burke, L.S. Chen, R.C. Clarke, P.M. Esker, H.M. Hobgood, R.H. Hopkins, A.W. Morse, L.B. Rowland, S. Seshadri, R.R. Siergiej, T.J. Smith, Jr. and S. Siriam, Tech. Dig. Inst. Electron. Dev. Meeting pp 9.1.1-9.1.6, Dec. 1996.

7. D.M. Brown, E. Downey, M. Ghezzo, J. Kretchmer, V. Krishnamurthy, W. Hennessy and G. Michon, Solid State Electron. 39 1531 (1996).

8. V.E. Chelnokov, Mat. Sci. Eng. B11 103 (1992).

9. T.P. Chow and M. Ghezzo, Mat. Res. Soc. Symp. Proc. 423 9 (1996).

10. S. Siriam, R.C. Clarke, A.A. Burk, Jr.H.M. Hobgood, P.G. McMullin, P.A. Orphanos, R.R. Siergiej, T.J. Smith, C.D. Brandt, M.C. Driver and R.H. Hopkins, IEEE Electron. Dev. Lett. 15 458 (1994).

11. K.E. Moore, C.E. Weitzel, K.J. Nordquist, L.L. Pond III, J.W. Palmour, S. Allen and C.H. Carter. Jr., IEEE Electron. Dev. Lett. 18 69 (1997).

12. J.W. Palmour, J.A. Edmond, H.S. Kong and C.H. Carter, Jr, Physica B 185 461 (1993).

13. J.B. Casady, D.C. Sheridan, W.C. Dillard and R.W. Johnson, Mat. Res. Soc.Symp. Proc. 423 105 (1996).

14. S.T. Sheppard, M.R. Melloch and J.A. Cooper, IEEE Trans. Electron. Dev. 41 1257 (1994).

15. J.B. Casady, J.D. Cressler, W.C. Dillard, R.W. Johnson, A.K. Agarwal and R.R. Siergiej, Solid State Electron. 39 777 (1996).

16. J.N. Sheroy, J.A. Cooper, Jr. and M.R. Melloch, IEEE Electron. Dev. Lett. 18 93 (1997).

17. A.K. Agarwal, R.R. Siergiej, M.H. White, P.G. McMullin, A.A. Burk, L.B. Rowland, C.D. Brandt and R.H. Hopkins, Mat. Res. Soc. Symp. Proc. 423 87 (1996).

18. P.G. Neudeck, D.J. Larkin, C.S. Salupo, J.A. Powell and L.G. Matus, Inst. Phys. Conf. Ser. 137 475 (1994).

19. O. Kordina, J.P. Bergman, A. Henry, E. Fanzen, S. Savage, J. Andre, L.P. Ramberg, U. Lindfelt, W. Hermanasson and K. Bergman, Appl. Phys. Lett. 67 1561 (1995).

20. M. Bhatnagar, P.K. McLarty and B.J. Baliga, IEEE Electron. Dev. Lett. 13 501 (1992).

21. W. Xie, J.A. Cooper, Jr. and M.R. Melloch, IEEE Electron. Dev. Lett. 15 455 (1994).

22. J.B. Casady and R.W. Johnson, Solid State Electron. 39 1409 (1996).

23. N.G. Hingorani and K.E. Stahlkopf, High-Power Electronics (Scientific American), 269 78-85, 1993.

24. M. Bhatnagar and B.J. Baliga, IEEE Transactions on Electron Devices, 40 645-655, 1993.

25. B.J. Baliga, Proceedings of the IEEE, 82 1112-1122, 1994.

26. R.J. Trew, J.-B. Yan, and P.M. Mock, Proceedings of the IEEE, 79 598-620, 1991.

27. W.C. Nieberding and J.A. Powell, IEEE Trans. on Industrial Electronics, 29 103-106, 1982.

28. S.J. Przybylko, Developments in Silicon Carbide for Aircraft Propulsion System Applications, American Institute of Aeronautics and Astronautics, Washington, DC, June 1993.

29. B. El-Kareh, Fundamentals of Semiconductor Processing Technology. Kluwer Academic Publishers, Boston, 1995.

30. D.J. Elliott, Integrated Circuit Fabrication Technology. McGraw-Hill, New York, 1982.

31. D.M. Manos and D.L. Flamm, Plasma Etching: An Introduction. Academic Press, Boston, 1989.

32. R.E. Williams, Gallium Arsenide Processing Techniques. Artech House Inc., Dedham, MA, 1984.

33. S.K. Ghandhi, VLSI Fabrication Principles. John wiley & Sons, Inc., New York, 1994.

34. J.W. Lee, Ph. D. dissertation, University of Florida, 1997.

35. O.A. Popov, High Density Plasma Sources: Design, Physics and Performance. Noyes Publications, Park Ridge, New Jersey, 1995.

36. G.C. Schwartz, K.V. Srikrishnan, and A. Bross, Handbook of Semiconductor Interconnection Technology. Marcel Dekker, Inc., New York, 1998.

37. S.J. Pearton, C.R. Abernathy and F. Ren, Appl. Phys. Lett. 64 2294 (1994).

38. CRC Handbook of Chemistry and Physics, 70th Edition. CRC Press, Boca Raton, FL, 1990.

39. R.J. Shul, G.B. McClellan, R.D. Briggs, D.J. Rieger, S.J. Pearton, C.R. Abernathy, J.W. Lee, C. Constantine and C. Barratt, J. Val. Sci. Technol. A 15 633 (1997).

40. S. Thomas III , K.K. Ko and S.W. Pang, J. Vac. Sci. Technol. A 13 894 (1995).

41. High Density Plasma Sources, ed. O.A. Popov. Noyes Publications, Park Ridge, NJ 1996.

42. U.K. Chakrabarti, S.J. Pearton and F. Ren, Semicond. Sci. Technol, 6 408 (1991).

43. D.T.C. Hou, M.F. Yan and J.D. Wynn, J. Electrochem. Soc. 137 3639 (1990).

44. I. Adesida, A. Mahajan, E. Andideh, M.A. Khan, D.J. Olson and J.W. Kuznia, Appl. Phys. Lett. 63 2777 (1993).

45. S.J. Pearton, R.J. Shul, G.F. McLane and C. Constantine, Solid State Electron. 41 159 (1997).

46. C.B. Vartuli, S.J. Pearton, J.W. Lee, J.D. Mackenzie, C.R. Abernathy, R.J. Shul, C. Constantine and C. Barratt, J. Electrochem. Soc. 144 2844 (1997)

47. D.L. Melville, J.G. Simmons and D.A. Thompson, J. Vac. Sci. Technol. B11 2038 (1993).

48. T. Matsui, H. Sugimoto, T. Ohnishi, K.Abe, K. Ohtsuka and H. Ogata, Appl. Phys.

Lett. 54 1193 (1989).

49. J.W. Lee and S.J. Pearton, Semicond. Sci. Technol. 11 812 (1996).

50. J.W. Lee, D. Hays, C.R. Abernathy, S.J. Pearton, W.S.Hobton and C. Constantine, J. Electrochem. Soc. 144 L245 (1997); J.W. Lee, C.R. Abernathy, S.J. Pearton, C. Constantine, R.J. Shul and W.S. Hobton, Plasma Sources Sci. Technol. 6 499 (1997).

51. K.B. Jung, E.S. Lambers, J.R. Childress, S.J. Pearton, M. Jenson and A.T. Hurst, Jr., Appl. Phys. Lett. 71 1255 (1997).

52. J.W. Lee and S.J. Pearton, Semicond. Sci. Technol. 11 812 (1996).

53. J.R. Flemish, K. Xie and J. Zhao, Appl. Phys. Lett. 64 2315 (1994).

54. J.R. Flemish and K. Xie, J. Electron. Soc. 143 2620 (1996).

55. J.R. Flemish, K. Xie and G.F. McLane, Mat. Res. Soc. Symp. Proc. 421 153 (1996).

56. M.A. Liebermann and A.J. Lichtenburg, Principles of Plasma Discharges and Materials Processing. Wiley & Sons, New York, 1994.

57. J.W. Lee, C.R. Abernathy, S.J. Pearton, R.J. Shul and C. Constantine, Plasma Sources Sci. Technol. 6 499 (1997).

58. K. Xie, J.R. Flemish, J.H. Zhao, W.R. Buchwald and L. Casas, Appl. Phys. Lett. 67 368 (1995).

BIOGRAPHICAL SKETCH

Juan-Juan Wang was born in Chengdu, China, on March 18, 1969. After high school, she went to the Chengdu University of Science and Technology, Chengdu, China, in 1986. She got a B. S. in Chemical Engineering from the university in 1990.

She was an assistant for six years in the Department of Chemical Engineering, Chengdu University of Science and Technology beginning in 1990.

She enrolled in the Graduate School, Chengdu University of Science and Technology, 1995, and was planning to get her M. S. degree in chemical engineering. However, she went to the United States and enrolled in the Graduate School, University of Florida in May, 1997. She is completing her M. S. degree in materials science and engineering in August, 1998 under Prof. Stephen J. Pearton. She is supposed to find a interesting and stimulating job in the semiconductor manufacturing field.

I certify that I have read this study and that in my opinion it conforms to acceptable standards of scholarly presentation and is fully adequate, in scope and quality, as a thesis for the degree of Master of Science.

Stephen J. Pearton, Chairman
Professor of Materials Science
and Engineering

I certify that I have read this study and that in my opinion it conforms to acceptable standards of scholarly presentation and is fully adequate, in scope and quality, as a thesis for the degree of Master of Science.

Cammy R. Abernathy
Professor of Materials Science
and Engineering

I certify that I have read this study and that in my opinion it conforms to acceptable standards of scholarly presentation and is fully adequate, in scopce and quality, as a thesis for the degree of Master of Science.

Rajiv K. Singh
Professor of Materials Science
and Engineering

This thesis was submitted to the Graduate Faculty of the College of Engineering and to the Graduate School and was accepted as partial fulfillment of the requirements for the degree of Master of Science.

August, 1998

Winfred M. Phillips
Dean, College of Engineering

Karen A. Holbrook
Dean, Graduate School